

Low-scale Leptogenesis with Minimal Lepton Flavour Violation

Matthew J. Dolan,* Tomasz P. Dutka,† and Raymond R. Volkas‡

University of Melbourne

Abstract

We analyse the feasibility of low-scale leptogenesis where the inverse seesaw (ISS) and linear seesaw (LSS) terms are not simultaneously present. In order to generate the necessary mass splittings, we adopt a Minimal Lepton Flavour Violation (MLFV) hypothesis where a sterile neutrino mass degeneracy is broken by flavour effects. We find that resonant leptogenesis is feasible in both scenarios. However, because of a flavour alignment issue, MLFV-ISS leptogenesis succeeds only with a highly tuned choice of Majorana masses. For MLFV-LSS, on the other hand, a large portion of parameter space is able to generate sufficient asymmetry. In both scenarios we find that the lightest neutrino mass must be of order 10^{-2} eV or below for successful leptogenesis. We briefly explore implications for low-energy flavour violation experiments, in particular $\mu \rightarrow e\gamma$. We find that the future MEG-II experiment, while sensitive to MLFV in our setup, will not be sensitive to the specific regions required for resonant leptogenesis.

* matthew.dolan@unimelb.edu.au

† tdutka@student.unimelb.edu.au; Corresponding Author

‡ raymondv@unimelb.edu.au

CONTENTS

I. Introduction	2
II. Model	6
A. MFV in the quark sector	6
B. MFV vs Experiment	8
C. MLFV	9
D. MLFV and the inverse and linear seesaw models	13
III. Leptogenesis	15
A. Baryon Asymmetry	18
IV. Numerical Results	21
A. Inverse seesaw (ISS)	27
B. $\ell_i \rightarrow \ell_j \gamma$ and MLFV-ISS	34
C. Linear Seesaw (LSS)	41
D. $\ell_i \rightarrow \ell_j \gamma$ and MLFV-LSS	46
V. Conclusion	49
Acknowledgments	52
References	52

I. INTRODUCTION

The type-I seesaw model [1–5] is the simplest known extension of the Standard Model (SM) that simultaneously addresses the origin of neutrino mass and the generation of the cosmological matter-antimatter asymmetry, the latter through thermal leptogenesis [6] (for reviews see [7–9]). One extra heavy Majorana sterile fermion is added per generation, where their masses are required to be higher than the critical temperature of the electroweak phase transition.

This scenario has been extensively studied and it has long been known that in the standard

hierarchical¹ type-I scenario of thermal leptogenesis, generation of the necessary asymmetry places a *lower-bound* [10, 11] on the heavy sterile neutrinos (SNs) of order 10^9 GeV. This prevents low-scale realisations of this model in its simplest form. However, an *upper-bound* [12, 13] can be placed on the SN neutrino mass of order 10^7 GeV by requiring that radiative corrections to the Higgs mass parameter μ^2 driven by the high seesaw scale does not exceed 1 TeV². A clear tension exists as there is no overlap between these two bounds. This can be resolved in a number of ways; by invoking supersymmetry to stabilise the Higgs mass, permitting a departure from strictly hierarchical heavy sterile neutrino masses [14, 15], adding a second Higgs doublet [16, 17] or adopting a modified lepton sector which allows for low-scale leptogenesis² from much lighter SN masses. Note that the first solution, while preventing large corrections, may generate other problems, e.g. cosmological gravitino over-production [18–20].

Lowering the thermal leptogenesis scale is an attractive and obvious way to resolve the above tension, and forms the basis of the present analysis. The scale of leptogenesis can be significantly lowered if a quasi-degenerate (meaning not exactly degenerate) spectrum of masses for the SNs is assumed [21, 22]. In the minimal type-I scenario this has the added consequence of suppressing the Yukawa couplings and therefore reducing discovery signals such as charged lepton flavour violation (cLFV). Additionally, a quasi-degeneracy should be motivated by some symmetry if such models are to be taken seriously. It is natural to expect that the origin of such a theory would tie in with the flavour problem of the SM.

A possible method of lowering the scale of thermal leptogenesis with potential cLFV signals is by introducing two SN states (with opposite lepton number assignments) per light neutrino and simultaneously promoting lepton number to being a “good symmetry” of the theory. For certain regimes of the couplings a double suppression of the active neutrino masses occurs, allowing significantly larger Yukawa couplings for SNs at TeV-scale masses compared to the minimal scenario. Additionally, due to the weakly broken lepton number symmetry, the heavy SNs form pseudo-Dirac states with mass splittings proportional to the small lepton number breaking terms. For specific choices of parameters, two popular limiting cases constitute the “inverse seesaw (ISS)” [23–30] and the “linear seesaw (LSS)” [31–34] models. The two cases can be linked by a rotation [35] only in the case where no additional

¹ Hierarchical is typically taken to mean $200m_{N_1} \lesssim m_{N_2} \lesssim m_{N_3}$.

² We define low-scale leptogenesis to occur at $\mathcal{O}(10 - 100$ TeV) or below.

symmetry precludes such a rotation (e.g. left-right or Pati-Salam symmetry [4, 36–39]). We will therefore be treating the two as independent scenarios in what follows.

In the specific case of the LSS above the electroweak phase transition, the heavy SNs are degenerate in mass and therefore self-energy diagrams vanish, leaving only the highly-suppressed vertex contributions to produce the CP asymmetry [40]. In the case of the ISS, a mass splitting does exist allowing for a resonant enhancement in the self-energy contribution for a specific choice of the mass splitting. However, decreasing the mass splitting also increases the efficiency of washout making asymmetry generation difficult in its simplest realisations [41–45] for ISS at the TeV scale.

In addition to the intra-family SN degeneracies, there is also the possibility of a quasi-degeneracy between SNs from different families, a flavour degeneracy in other words. To that end we explore a scenario in which an $SU(3)^2 \times SO(3)^2$ flavour symmetry, to be defined below, is utilised in the lepton sector. Due to the $SO(3)$ symmetry, mass terms for the heavy SNs are proportional to the identity matrix and lead to a flavour degeneracy amongst the SN states in both the ISS and LSS scenarios. However, radiative effects induce $SO(3)$ -breaking terms which in turn break these degeneracies, enabling a resonant enhancement in the asymmetry generation for both the LSS and ISS scenarios.

We work in the framework of an extended version of the Minimal Lepton Flavour Violation (MLFV) [46, 47] scenario, which is itself an extension of the well-established idea of Minimal Flavour Violation (MFV) within the quark sector [48–50]. The MFV scheme is an ansatz designed to address the very stringent bounds placed on new physics from various rare hadronic decays and neutral meson oscillations. It is motivated by the idea that taking the Yukawa sector couplings to zero recovers five separate³ flavour space rotations which leave the Lagrangian invariant. Therefore an MFV or MLFV Ansatz is based on the core principle that these are “good” flavour symmetries which are broken *solely* by the SM Yukawa fields.

Under this ansatz, Yukawa couplings are said to arise from dynamical fields typically known as ‘spurions’ which transform under the flavour symmetries such that the Lagrangian is flavour invariant. These spurion fields are taken to have non-zero vacuum expectation values (VEVs) which spontaneously break the flavour symmetries and thereby induce the masses and flavour mixing we observe. As a result, in its most minimal realisation, any flavour changing process can be predicted from the well-measured Cabibbo-Kobayashi-Maskawa

³ In the absence of neutrino mass. If neutrino mass is included more rotations are present.

(CKM) mixing matrix and the fermion masses.

Due to the multiple distinct ways in which neutrino masses can be incorporated into the SM there is no unique way of defining an MLFV Ansatz, in contrast with MFV in the quark sector. The potential connection between an MLFV Ansatz and resonant leptogenesis⁴ has been identified previously [52–54] in the type-I seesaw context. Since then it has been discovered that, due to developments within flavoured leptogenesis, there is a significant reduction in the allowed parameter space⁵ [55–57] specific to MLFV leptogenesis. Additionally, in order to produce large leptonic flavour violation whilst suppressing neutrino masses in such models, a separation between the scale of lepton-number violation (LNV) and lepton-flavour violation (LFV) should exist which is not present in the type-I seesaw alone [53, 58]. Neither of these issues are present for MLFV in the ISS and LSS, allowing the possibility of MLFV-induced resonant leptogenesis in these scenarios. We assume an ansatz such that the heavy sterile Majorana neutrinos introduced have exactly degenerate masses in the Lagrangian, motivated by the flavour symmetry of the theory. Radiative effects will break this down to a quasi-degeneracy between the SNs from which a resonant enhancement in the asymmetry generated per decay of SN will occur. For some choices of parameters which we will identify, this enhancement is able to generate the necessary baryon asymmetry observed in the universe. We will explore the viability of leptogenesis both from PMNS phases (particularly the Dirac phase) alone [43, 59–61] as well as from CPV parameters related to the heavy SNs.

This paper is organised as follows. Section II reviews the basic idea behind the MFV and MLFV Ansätze including justification from hadronic observables for the MFV hypothesis. Section III describes our technique for calculation of the baryon asymmetry in the ISS and LSS models with MLFV, while Sec. IV provides a description of our choice of scans and a discussion of the results. Here we also briefly assess the discovery potential of these models at current and future cLFV experiments. We conclude in Sec. V.

⁴ See [51] for an example of an MLFV Ansatz which incorporates leptogenesis without resonance effects.

⁵ Recently it was found that flavour effects can still be relevant at much higher temperatures than thought previously, potentially reducing the allowed parameters space even further [15].

	$U(1)_B$	$U(1)_{A^u}$	$U(1)_{A^d}$	$SU(3)_{q_L}$	$SU(3)_{u_R}$	$SU(3)_{d_R}$
q_L	1/3	1	1	3	1	1
u_R	1/3	-1	0	1	3	1
d_R	1/3	0	-1	1	1	3

TABLE I: Representations of the SM quark fields under the Abelian and non-Abelian parts of \mathcal{G}^Q which leave the kinetic terms of the SM Lagrangian invariant.

II. MODEL

A. MFV in the quark sector

The Minimal Flavour Violation ansatz [48–50] recognises that, in the massless limit of absent Yukawa couplings, the quark sector of the three-family SM is invariant under a product of $U(3)$ flavour groups, where an individual $U(3)$ acts in flavour space on a given type of SM multiplet: q_L , u_R and d_R . Utilising $U(3) = SU(3) \times U(1)$, the quark-sector flavour group may be expressed as

$$\mathcal{G}^Q = \underbrace{U(1)_B \times U(1)_{A^u} \times U(1)_{A^d}}_{\mathcal{G}_A^Q} \times \underbrace{SU(3)_{q_L} \times SU(3)_{u_R} \times SU(3)_{d_R}}_{\mathcal{G}_{NA}^Q}. \quad (1)$$

The Abelian transformations are flavour-blind and we have the freedom to identify them with baryon number and two axial rotations [62]. The non-Abelian transformations do act in flavour space; they govern interactions between the different flavours and hence are responsible for the flavour violation in the theory. Table I defines the representations of the SM quark fields under the flavour symmetries and specifies a basis for the Abelian generators.

The Yukawa terms in the SM are not invariant under these flavour transformations, but can be made invariant if the Yukawa matrices are ‘promoted’ to be *spurionic* fields.⁶ Unique transformations under the flavour symmetries are assigned to the spurions in order to make the would-be flavour-breaking terms invariant. This is a hypothesis motivated by the lack of experimental evidence for new flavour-violating physics; it should be treated as

⁶ In this work, promoting a Yukawa coupling to be a dynamical field will be represented by $Y_i \rightarrow \mathcal{Y}_i$.

the low-energy limit of an unspecified higher-scale, renormalisable theory. The necessary transformations under the non-Abelian symmetries are summarised in table II.

Quark masses are generated in this framework when the spurionic fields acquire nonzero VEVs alongside the SM Higgs doublet. These background values relate to the *physically measurable* quark masses and mixings where we have the freedom to choose a basis such that

$$\langle \mathcal{Y}_u \rangle = \frac{\sqrt{2}}{v} V_{\text{CKM}}^\dagger \hat{m}_u \quad \text{and} \quad \langle \mathcal{Y}_d \rangle = \frac{\sqrt{2}}{v} \hat{m}_d \quad (2)$$

where

$$\hat{m}_u = \text{diag}(m_u, m_c, m_t) \quad \text{and} \quad \hat{m}_d = \text{diag}(m_d, m_s, m_b), \quad (3)$$

V_{CKM} is the quark mixing matrix measured by experiment and here, by the usual convention, we have chosen the VEVs of the spurion fields such that the down-type matrix is diagonal and the up-type is not.

The MFV ansatz is based on two assumptions about the high-scale, renormalisable theory:

- The flavour symmetry present in the SM quark kinetic terms is a ‘good’ symmetry which the high-scale sector respects. The *only* sources of flavour symmetry breaking within the theory at the high scale are from the VEVs of the Yukawa coupling spurions.⁷ The dynamics by which these VEVs are generated lie in the unspecified high-scale theory.
- The SM is an effective theory for which all renormalisable and non-renormalisable operators must respect both the gauge and *flavour* symmetries of the theory. All operators which are not formally invariant under the flavour symmetry are made so by insertions of the appropriate combinations of Yukawa fields.

A number of consequences follow from this ansatz.

SM effective field theory operators which describe flavour changing processes require insertions of spurion combinations in order to become flavour invariant. For example, the four fermion operator $(\overline{Q}_L \gamma_\mu Q_L)(\overline{Q}_L \gamma^\mu Q_L)$ is forced to be flavour preserving by the flavour symmetry. In order to get a related $\Delta F = 1$ operator, a spurion insertion must be made: $\mathcal{O}_{q1} = (\overline{Q}_L \mathcal{Y}_u \mathcal{Y}_u^\dagger \gamma_\mu Q_L)(\overline{Q}_L \gamma^\mu Q_L)$ is flavour invariant due to the insertion of $\mathcal{Y}_u \mathcal{Y}_u^\dagger$, but gives

⁷ Therefore under this Ansatz flavour violation is completely dictated by the flavour structure of the Yukawa terms in the Lagrangian; any new physics introduced into the theory should not contribute to flavour-changing processes.

	$SU(3)_{q_L}$	$SU(3)_{u_R}$	$SU(3)_{d_R}$
\mathcal{Y}_u	3	$\bar{3}$	1
\mathcal{Y}_d	3	1	$\bar{3}$

TABLE II: Representation assignments for Yukawa spurions such that the Yukawa terms in the MFV effective theory respect the flavour symmetry which exists in their absence.

rise to flavour-changing processes when the spurions acquire VEVs. Due to the hierarchy of the couplings within \mathcal{Y}_u there is an in-built suppression of flavour-changing processes for the first two generations of quarks. A list of relevant spurion insertions for operators involving fermions at dimension six can be found in [50].

Of particular importance when adapted to resonant leptogenesis, which will be discussed in more detail later, all terms in the lowest-order MFV Lagrangian will receive corrections to their couplings from spurion terms which transform in the same way as the basic spurion under the flavour symmetry. For example, in

$$\overline{Q_L} \left(\mathcal{Y}_d + \epsilon_1 \mathcal{Y}_d \mathcal{Y}_d^\dagger \mathcal{Y}_d + \dots \right) d_R H, \quad (4)$$

the higher-order term $\mathcal{Y}_d \mathcal{Y}_d^\dagger \mathcal{Y}_d$ transforms in the same way as \mathcal{Y}_d and therefore under the ansatz has to be included. As Yukawa spurion VEVs are small in magnitude these corrections are generally not significant.

B. MFV vs Experiment

The motivation behind adopting the MFV ansatz is due to the strong limits placed on the mass scale of new physics from flavour-violating hadronic processes involving the first generation, as illustrated in table III. If new physics appears at scales lower than these bounds it would indicate that either flavour violation arises solely, or dominantly, due to the SM CKM matrix indicating an MFV-like theory, or that it could couple dominantly to the heavier generations which have less stringent bounds.

A key advantage of the former assumption is that strict relations between different flavour changing processes arise due to precise measurements of the CKM parameters. Therefore

Hadronic Process Bound on Λ_{NP}	
$K^0 - \overline{K^0}$	9×10^3 TeV
$B_d - \overline{B_d}$	4×10^2 TeV
$B_s - \overline{B_s}$	7×10^1 TeV

TABLE III: Approximate lower bounds on the scale Λ_{NP} of new physics from precision measurements of neutral meson oscillations assuming dimension six and $\mathcal{O}(1)$ Wilson coefficients [63]. The bounds are stronger when first-generation quarks are involved.

MFV-like theories have a degree of predictivity which can aid experimental searches. In the case of an exact MFV ansatz, relations amongst different flavour transitions, e.g. $b \rightarrow s, b \rightarrow d$ and $s \rightarrow d$, can be used to make predictions of unmeasured (or poorly measured) observables [64–66], some of which are summarised in table IV. They can be compared to their corresponding experimental measurement or limit [67–71] showing strong correlation.

Most channels have measurements (or upper limits) in agreement with MFV predictions, however a discrepancy exists for $B_d \rightarrow \mu^+ \mu^-$ between the CMS/LHCb [68] and ATLAS [71] collaborations. CMS/LHCb measure the rate for this process at the limit of the MFV prediction, whereas ATLAS place an upper-bound consistent with MFV. More precise measurements are required and could potentially suggest a deviation from an exact MFV theory. Certainly, however, we have strong evidence that flavour violation is dominantly generated by the Yukawa couplings.

C. MLFV

While the MFV ansatz for the quark sector can be uniquely implemented (with strong agreement with measurement) there is an issue when extending this concept to leptons. Currently we do not know the origin of LFV and most importantly whether the light neutrinos are predominantly Dirac or Majorana. One may expand the MFV ansatz to the lepton sector, which is termed MLFV, but a dependence exists on the specific SM extension adopted for neutrino mass generation and a freedom exists in choosing which couplings are flavour vi-

Hadronic Process Measured value or upper limit MFV prediction		
$\mathcal{A}_{CP}(B \rightarrow X_s \gamma)$	$0.0144^{+0.0139}_{-0.0139}$	< 0.02
$\mathcal{B}(K_L \rightarrow \pi^0 \nu \bar{\nu})$	$< 2.6 \times 10^{-10}$	$< 2.9 \times 10^{-10}$
$\mathcal{B}(B \rightarrow X_s \tau^+ \tau^-)$	-	$[0.2, 3.7] \times 10^{-7}$
$\mathcal{B}(B \rightarrow X_d \gamma)$	$(1.41^{+0.57}_{-0.57}) \times 10^{-5}$	$[1.0, 4.0] \times 10^{-5}$
$\mathcal{B}(B_d \rightarrow \mu^+ \mu^-)$	$(0.39^{+0.16}_{-0.14} \times 10^{-9})_{\text{CMS/LHCb}}$	$< 0.38 \times 10^{-9}$
	$< (0.21 \times 10^{-9})_{\text{ATLAS}}$	

TABLE IV: Predictions for some rare hadronic observables under the MFV ansatz [64–66], based on other precisely measured processes, compared with their current experimental limits [67–71].

olating [72]. The simplest approach is to extend the SM by three right-handed neutrinos N_R in the usual way where lepton number violation occurs through gauge-invariant Majorana neutrino mass terms,

$$\mathcal{L}_{\text{SEESAW}} = \mathcal{L}_{\text{ss}}^{\text{K}} - \mathcal{L}_{\text{ss}}^{\text{M}}, \quad (5)$$

where $\mathcal{L}_{\text{ss}}^{\text{K}}$ is the usual kinetic term and

$$\mathcal{L}_{\text{ss}}^{\text{M}} = \epsilon_e \bar{\ell}_L Y_e e_R H + \epsilon_D \bar{\ell}_L Y_D N_R \tilde{H} + \frac{1}{2} \mu_N \overline{N_R^c} Y_N N_R + \text{h.c.} \quad (6)$$

The *numbers* $\epsilon_{e,D}$ and μ_N are to be distinguished from the *matrices* (in flavour space) $Y_{e,D,N}$ which will ultimately act as sources for the breaking of the Abelian and non-Abelian flavour symmetries respectively once promoted to spurions having non-zero VEVs.

Similar to the quarks and MFV, the gauge sector of the leptons obey a flavour-transformation invariance which can be defined analogously to eq. (1),

$$\mathcal{G}^L = \underbrace{U(1)_L \times U(1)_{A^e} \times U(1)_{A^N}}_{\mathcal{G}_A^L} \times \underbrace{SU(3)_{\ell_L} \times SU(3)_{e_R} \times SU(3)_{N_R}}_{\mathcal{G}_{\text{NA}}^L}. \quad (7)$$

In the absence of $\mathcal{L}_{\text{ss}}^{\text{M}}$, the Lagrangian is invariant under the following $SU(3)$ rotations

$$\ell_L \rightarrow \mathcal{U}_{\ell_L} \ell_L \quad e_R \rightarrow \mathcal{U}_{e_R} e_R \quad N_R \rightarrow \mathcal{U}_{N_R} N_R \quad (8)$$

implying the following representations for the fields:

$$\ell_L \sim (\mathbf{3}, \mathbf{1}, \mathbf{1}) \quad e_R \sim (\mathbf{1}, \mathbf{3}, \mathbf{1}) \quad N_R \sim (\mathbf{1}, \mathbf{1}, \mathbf{3}). \quad (9)$$

Once again, flavour invariance can be recovered (once \mathcal{L}_{ss}^M is reintroduced) by promoting the relevant couplings to spurions with fixed transformation properties under the flavour symmetries,

$$\mathcal{Y}_e \rightarrow \mathcal{U}_{\ell_L} \mathcal{Y}_e \mathcal{U}_{e_R}^\dagger \quad \mathcal{Y}_D \rightarrow \mathcal{U}_{\ell_L} \mathcal{Y}_D \mathcal{U}_{N_R}^\dagger \quad \mathcal{Y}_N \rightarrow \mathcal{U}_{N_R}^* \mathcal{Y}_N \mathcal{U}_{N_R}^\dagger \quad (10)$$

implying the following representations for the fields

$$\mathcal{Y}_e \sim (\mathbf{3}, \overline{\mathbf{3}}, \mathbf{1}) \quad \mathcal{Y}_D \sim (\mathbf{3}, \mathbf{1}, \overline{\mathbf{3}}) \quad \mathcal{Y}_N \sim (\mathbf{1}, \mathbf{1}, \overline{\mathbf{6}}). \quad (11)$$

Lepton masses and mixings appear once these spurionic fields acquire non-zero VEVs along with the SM Higgs. We are free to choose a basis such that

$$\langle \mathcal{Y}_e \rangle = \frac{\sqrt{2}}{v} \hat{m}_\ell, \quad \langle \mathcal{Y}_D \rangle \langle \mathcal{Y}_N^{-1} \rangle \langle \mathcal{Y}_D^T \rangle = \frac{2\mu_N}{v^2} U_{\text{PMNS}} \hat{m}_\nu U_{\text{PMNS}}^T \quad (12)$$

where

$$\hat{m}_\ell = \text{diag}(m_e, m_\mu, m_\tau), \quad \hat{m}_\nu = \text{diag}(m_{\nu_1}, m_{\nu_2}, m_{\nu_3}). \quad (13)$$

It is clear from eq. (12) that it is not possible to assign unique background values to the spurions \mathcal{Y}_D and \mathcal{Y}_N in terms of physically measurable parameters. Rather, it is the combination in the seesaw formula that is fixed by the physical observables. As a consequence each individual spurion cannot be uniquely written in terms of physical masses and mixings. In the quark sector, under the MFV ansatz, higher-dimensional operators which control rare processes are made flavour invariant from the necessary combination of spurion fields. As their background values are only dependent on quark sector masses and mixings, this prevents any sources of new physics from contributing in a way not aligned with the SM flavour violation. For the lepton sector, however, rare flavour-violating processes will not in general be made invariant by the exact combination $\mathcal{Y}_D \mathcal{Y}_N^{-1} \mathcal{Y}_D^T$, but through different combinations of these two spurions (see [47] for a list of examples). Therefore specific flavour-changing processes cannot be uniquely written in terms of physically measurable parameters in the same way they can be for MFV.

Predictivity can be recovered if only one of the spurion fields is taken to have non-trivial flavour transformations, with the other not acting as a source of flavour-symmetry breaking.

Usually, it is assumed that the Majorana mass term does not act as a source of lepton-flavour breaking and, and as in the quark sector, only the Yukawa couplings are responsible. If it is assumed that the Majorana mass term is lepton-flavour blind, then Y_N must necessarily be equal to the identity matrix (in flavour space). Under this assumption the non-Abelian flavour symmetry of the theory⁸ reduces to

$$\mathcal{G}_{\text{NA}}^L = SU(3)_{\ell_L} \times SU(3)_{e_R} \times SO(3)_{N_R} \times CP. \quad (14)$$

The lepton-flavour symmetry is broken by \mathcal{Y}_D and \mathcal{Y}_e which can now be written uniquely in terms of lepton masses and mixings

$$\langle \mathcal{Y}_e \rangle = \frac{\sqrt{2}}{v} \hat{m}_\ell, \quad \langle \mathcal{Y}_D \rangle \langle \mathcal{Y}_D^T \rangle = \frac{2\mu_N}{v^2} U_{\text{PMNS}} \hat{m}_\nu U_{\text{PMNS}}^T, \quad \langle \mathcal{Y}_N \rangle = \mathbb{1}_3. \quad (15)$$

The measured masses and mixings in the lepton sector fix the combination $\mathcal{Y}_D \mathcal{Y}_D^T$ in this setup and not the spurion \mathcal{Y}_D itself. However, often the combination $\mathcal{Y}_D \mathcal{Y}_D^\dagger$ (which transforms as a **(8,1,1)** under \mathcal{G}^L) is required to be inserted for many operators. Without the imposition of CP invariance, additional and yet unmeasured phases will appear in the predictions for flavour-changing processes. However, in general we expect CP violation (CPV) to be present in the lepton sector.

Allowing for leptonic CPV, as necessary for leptogenesis, a slightly less minimal flavour ansatz is required, namely

$$\mathcal{G}_{\text{NA}}^L = SU(3)_{\ell_L} \times SU(3)_{e_R} \times SO(3)_{N_R}. \quad (16)$$

Lifting the assumption of CP invariance introduces new non-SM phases, as well as allowing non-trivial phases in the Pontecorvo-Maki-Nakagawa-Sakata (PMNS) mixing matrix. While they spoil the absolute predictivity of the theory, they generally lead to only small deviations in cLFV observables [52–54]. This is not in conflict with experiment (as it might be in the quark sector) as currently no cLFV processes have been measured. Additionally, although not definitive, there is interesting evidence for CPV in neutrino oscillations [74] motivating the less-minimal definition of the MLFV principle where phases are allowed and their effect on measurable processes are taken into account.

⁸ A alternative approach is to assume $\mathcal{G}_{\text{NA}}^L = SU(3)_{V=(\ell_L+N_R)} \times SU(3)_{e_R}$ and then via Schur's Lemma one of the flavour space matrices must be unitary which can be rotated to the identity matrix with a field redefinition. Under this assumption no degeneracy is implied amongst the right-handed neutrinos and CP invariance is not necessary. [73]

As already emphasised, MFV and MLFV should be understood as hypotheses motivated by experiment and do not provide a complete UV description of the flavour sector. Attempts have been made in moving from this ansatz to a renormalisable model. In particular in the case of the simplest type-I MLFV Ansatz, the spurion scalar potentials have been studied [75–77] with suggestive conclusions. For hierarchical masses amongst the charged leptons, *large* mixing angles appear when Majorana neutrinos are considered, whereas in the quark sector *small* mixing angles are predicted. It has been suggested that the disparity in the mixing between the lepton and quark sector is therefore due to the Majorana properties of the right-handed neutrinos. These results suggest that UV completions of the MFV and MLFV Ansätze could ultimately explain the origin of the flavour structure of the SM.

D. MLFV and the inverse and linear seesaw models

It was noted in [46, 53, 58] that in order to generate measurable LFV effects whilst explaining the smallness of the active neutrino masses, a decoupling between the LFV scale and LNV scale is required such that $\Lambda_{\text{LFV}} \ll \Lambda_{\text{LN}}$. This observation, coupled with any future measurement of cLFV, motivates the incorporation of such a scale separation into the MLFV hypothesis. Note that LNV arises from the breaking of Abelian symmetries in eq. (7), whereas LFV arises from the breaking of the non-Abelian symmetries.

Scale separation, however, does not occur in the minimal version of the type-I and type-III seesaw mechanisms where only one new scale is introduced such that $\Lambda_{\text{LFV}} = \Lambda_{\text{LN}} = \mu_N$. Under an MLFV Ansatz the flavour spurions decouple when the LNV scale is taken to infinity [58], preventing significant LFV. In contrast it was argued that the type-II seesaw does exhibit such a behaviour as $\Lambda_{\text{LN}} \sim M_\Delta^2/\mu_\Delta$ while $\Lambda_{\text{LFV}} \sim M_\Delta$, where M_Δ is the mass of the triplet and μ_Δ is the dimensionful cubic coupling constant between the triplet and the SM Higgs doublet. This therefore defines the only minimal seesaw model for which an MLFV Ansatz may lead to significant LFV.

The simplest⁹ *fermionic* completion which achieves a natural scale separation features in the ISS and LSS mechanisms (and a combination of the two) where small LNV parameters are introduced in order to ensure an *approximate* $U(1)_L$ symmetry. Here additional sterile

⁹ In [53] it was suggested the two scales could be made distinct by implementing the minimal type-I seesaw mechanism through an extended theory such as the MSSM, where $\Lambda_{\text{LFV}} = m_{\tilde{\ell}} \sim \mathcal{O}(\text{TeV})$ is proportional to the soft-SUSY breaking terms.

neutrino degrees of freedom S_L are introduced alongside the right-handed neutrinos N_R ,

$$\mathcal{L}_{\text{ESS}} = \mathcal{L}_{\text{ESS}}^{\text{K}} - \mathcal{L}_{\text{ESS}}^{\text{M}}, \quad (17)$$

$$\begin{aligned} \mathcal{L}_{\text{ESS}}^{\text{M}} = & \epsilon_e \overline{\ell_L} \mathcal{Y}_e H e_R + \epsilon_D \overline{\ell_L} \mathcal{Y}_D \tilde{H} N_R + \epsilon_L \overline{\ell_L} \mathcal{Y}_L \tilde{H} (S_L)^c + m_R \overline{(N_R)^c} \mathcal{Y}_R (S_L)^c \\ & + \frac{1}{2} \mu_S \overline{S_L} \mathcal{Y}_{\mu_S} (S_L)^c + \frac{1}{2} \mu_N \overline{(N_R)^c} \mathcal{Y}_{\mu_N} N_R + \text{h.c.} \end{aligned} \quad (18)$$

where it is conventional to choose $L(\ell_L) = L(N_R) = 1$ and $L(S_L) = -1$.

As before, \mathcal{Y}_i correspond to dimensionless 3×3 matrices in flavour space associated with the breaking of $\mathcal{G}_{\text{NA}}^L$. We impose an $SO(3)$ rather than $SU(3)$ flavour invariance for the heavy singlets to ensure that only the Yukawa interactions with the Higgs doublet act as sources of flavour-symmetry breaking. Therefore all bare mass terms related to the heavy singlets are proportional to the identity matrix. The flavour symmetry of the theory is defined analogously to eq. (7),

$$\mathcal{G}^L = \underbrace{U(1)_L \times U(1)_{A^e} \times U(1)_{A^N} \times U(1)_{A^S}}_{\mathcal{G}_A^L} \times \underbrace{SU(3)_{\ell_L} \times SU(3)_{e_R} \times SO(3)_{N_R} \times SO(3)_{S_L}}_{\mathcal{G}_{\text{NA}}^L}. \quad (19)$$

The mass matrix has the form

$$M_\nu = \begin{pmatrix} 0 & \frac{1}{\sqrt{2}} \epsilon_D \mathcal{Y}_D v & \frac{1}{\sqrt{2}} \epsilon_L \mathcal{Y}_L v \\ \frac{1}{\sqrt{2}} \epsilon_D \mathcal{Y}_D^T v & \mu_N \mathcal{Y}_{\mu_N} & m_R \mathcal{Y}_R \\ \frac{1}{\sqrt{2}} \epsilon_L \mathcal{Y}_L^T v & m_R \mathcal{Y}_R & \mu_S \mathcal{Y}_{\mu_S} \end{pmatrix} \quad (20)$$

where for the ISS ($\epsilon_L = 0$)

$$\Lambda_{\text{LNV}} \sim \frac{m_R^2}{\mu} \quad \text{and} \quad \Lambda_{\text{LFV}} \sim m_R \quad (21)$$

and for the LSS ($\mu_N, \mu_S = 0$)

$$\Lambda_{\text{LNV}} \sim \frac{m_R}{\sqrt{\epsilon_L}} \quad \text{and} \quad \Lambda_{\text{LFV}} \sim m_R. \quad (22)$$

The imposition of small lepton number violation means that μ_S, μ_N and ϵ_L are small. This provides the desired separation of scales.

As with the quark sector and the example of the minimal type-I seesaw model, the kinetic terms in eq. (17) are invariant under the following flavour rotations

$$\ell_L \rightarrow \mathcal{U}_{\ell_L} \ell_L \quad e_R \rightarrow \mathcal{U}_{e_R} e_R \quad N_R \rightarrow \mathcal{O}_{N_R} N_R \quad S_L \rightarrow \mathcal{O}_{S_L} S_L \quad (23)$$

where \mathcal{U}_i are 3×3 special unitary matrices, \mathcal{O}_i are 3×3 real-orthogonal matrices and for example $\ell_L = (e_L, \mu_L, \tau_L)$. The leptons transform as fundamentals under their respective non-Abelian rotations

$$\ell_L \sim (\mathbf{3}, \mathbf{1}, \mathbf{1}, \mathbf{1}) \quad e_R \sim (\mathbf{1}, \mathbf{3}, \mathbf{1}, \mathbf{1}) \quad N_R \sim (\mathbf{1}, \mathbf{1}, \mathbf{3}, \mathbf{1}) \quad S_L \sim (\mathbf{1}, \mathbf{1}, \mathbf{1}, \mathbf{3}). \quad (24)$$

It follows that eq. (18) can be made invariant by promoting the relevant couplings to dynamical spurions with the flavour transformation properties,

$$\mathcal{Y}_e \rightarrow \mathcal{U}_{\ell_L} \mathcal{Y}_e \mathcal{U}_{e_R}^\dagger \quad \mathcal{Y}_D \rightarrow \mathcal{U}_{\ell_L} \mathcal{Y}_D \mathcal{O}_{N_R}^T \quad \mathcal{Y}_L \rightarrow \mathcal{U}_{\ell_L} \mathcal{Y}_L \mathcal{O}_{S_L}^T \quad (25)$$

implying that

$$\mathcal{Y}_e \sim (\mathbf{3}, \bar{\mathbf{3}}, \mathbf{1}, \mathbf{1}) \quad \mathcal{Y}_D \sim (\mathbf{3}, \mathbf{1}, \mathbf{3}, \mathbf{1}) \quad \mathcal{Y}_L \sim (\mathbf{3}, \mathbf{1}, \mathbf{1}, \mathbf{3}). \quad (26)$$

Lepton masses and mixings result as usual from non-zero VEVs for the spurion fields where, similarly to eq. (12), a basis can be chosen such that

$$\langle \mathcal{Y}_e \rangle = \frac{\sqrt{2}}{v} \hat{m}_\ell \quad \langle \mathcal{Y}_D \rangle \langle \mathcal{Y}_D^T \rangle = \frac{2 m_R^2}{v^2 \mu_S} U_{\text{PMNS}} \hat{m}_\nu U_{\text{PMNS}}^T \quad (27)$$

in the case of the inverse seesaw and

$$\langle \mathcal{Y}_e \rangle = \frac{\sqrt{2}}{v} \hat{m}_\ell \quad \langle \mathcal{Y}_D \rangle \langle \mathcal{Y}_L^T \rangle + \langle \mathcal{Y}_L \rangle \langle \mathcal{Y}_D^T \rangle = \frac{2 m_R}{v^2 \epsilon_L} U_{\text{PMNS}} \hat{m}_\nu U_{\text{PMNS}}^T \quad (28)$$

in the case of the linear seesaw.

III. LEPTOGENESIS

The leading-order flavour degeneracy amongst the heavy SNs is built into the ansatz, with higher order spurion effects breaking the degeneracy. This allows for a resonant enhancement in asymmetry generation.

The case of the simplest MLFV scenario has been explored in detail [52–54, 78]. Recent developments related to flavoured leptogenesis [55–57] have, however, highlighted the importance of a term not previously included, such that the flavoured CP-asymmetry is proportional to

$$\epsilon_i^\alpha \propto 2 \sum_{j \neq i} \text{Im} \left\{ (\mathcal{Y}_D)_{\alpha i} (\mathcal{Y}_D)_{\alpha j} \right\} \text{Re} \left\{ (\mathcal{Y}_D^\dagger \mathcal{Y}_D)_{ij} \right\} + \mathcal{O}(\mathcal{Y}_D^6). \quad (29)$$

Equation 29 requires the existence of real, off-diagonal entries in $\mathcal{Y}_D^\dagger \mathcal{Y}_D$ in order for non-zero asymmetry generation to appear at lowest order in the couplings. It turns out that this presents a problem, as we now review, and provides an independent motivation for the ISS and LSS extended seesaw schemes in the MLFV and leptogenesis context.

In the case of the MLFV Ansatz implemented in the type-I seesaw scenario, the radiative corrections to the SN Majorana masses are incorporated through

$$\tilde{\mu}_N = \mu_N \mathbb{1}_3 + \delta\mu_N, \quad (30)$$

where μ_N is defined in eq. (6) and the $SO(3)$ breaking source $\delta\mu_N$ arises from all spurion insertions that transform such that the combination $\overline{N_R^c} \delta\mu_N N_R$ starts off flavour invariant. From here on, Majorana masses with tildes will denote that corrections have been included whereas without will denote the $SO(3)$ conserving bare mass. At lowest order they are

$$\begin{aligned} \delta\mu_N &= \mu_N \left[n_1 \left(\mathcal{Y}_D^\dagger \mathcal{Y}_D + \mathcal{Y}_D^T \mathcal{Y}_D^* \right) \right] \\ &= 2\mu_N n_1 \operatorname{Re} \left\{ \mathcal{Y}_D^\dagger \mathcal{Y}_D \right\} \end{aligned} \quad (31)$$

where n_1 is a Wilson coefficient which at the effective level is a free parameter. The two terms appearing in eq. (31) can be checked to transform in the appropriate way by applying the rotations defined in eqs. (24) and (25) to the terms of eq. (31). For the MLFV Ansatz these terms must be included, but we remain agnostic as to how they are generated.

In order to calculate the CP-asymmetry one must first rotate the SN into their mass basis. The unitary matrix responsible for diagonalising the heavy SNs in this case is real (and therefore orthogonal):

$$\begin{pmatrix} 0 & m_D \\ m_D^T & \mu_N \mathbb{1}_3 + \delta\mu_N \end{pmatrix} \rightarrow \begin{pmatrix} 0 & m_D \mathcal{O} \\ \mathcal{O}^T m_D^T & \mathcal{O}^T (\mu_N \mathbb{1}_3 + \delta\mu_N) \mathcal{O} \end{pmatrix} = \begin{pmatrix} 0 & m_D \mathcal{O} \\ \mathcal{O}^T m_D^T & \hat{\tilde{\mu}}_N \end{pmatrix} \quad (32)$$

where $\hat{\tilde{\mu}}_N = \operatorname{diag}(\mu_N + \delta_1, \mu_N + \delta_2, \mu_N + \delta_3)$. Due to the degeneracy required in \mathcal{Y}_N and the allowed flavour invariant terms of eq. (31) the rotation matrix \mathcal{O} is exactly the matrix which diagonalizes $\operatorname{Re} \left\{ \mathcal{Y}_D^\dagger \mathcal{Y}_D \right\}$. Therefore the CP asymmetry for flavoured leptogenesis shifts to

$$\operatorname{Re} \left\{ \mathcal{Y}_D^\dagger \mathcal{Y}_D \right\} \rightarrow \operatorname{Re} \left\{ \mathcal{O}^T \mathcal{Y}_D^\dagger \mathcal{Y}_D \mathcal{O} \right\} = \mathcal{O}^T \operatorname{Re} \left\{ \mathcal{Y}_D^\dagger \mathcal{Y}_D \right\} \mathcal{O} = \operatorname{diag}(\dots) \quad (33)$$

which has no off-diagonal terms and thus the CP asymmetry vanishes exactly. A non-zero asymmetry could potentially be recovered by including higher-order terms of $\mathcal{O}(\mathcal{Y}_D^6)$ of

appropriate form. However, due to the suppression from the additional powers of couplings in the assumed perturbative regime, a substantial asymmetry will be difficult to generate even if resonance effects are present.

Alternatively, the consideration of higher-order corrections to the Majorana mass which are not all aligned in flavour space will cause non-zero real entries in the relevant term of eq. (29). Higher-order terms which transform in the same way as in eq. (31) can be constructed from the charged-lepton spurion, as per

$$\delta\mu_N = \mu_N \left[c_1 \left(\mathcal{Y}_D^\dagger \mathcal{Y}_D + \mathcal{Y}_D^T \mathcal{Y}_D^* \right) + \dots + c_i \left(\mathcal{Y}_D^\dagger \mathcal{Y}_e \mathcal{Y}_e^\dagger \mathcal{Y}_D + \mathcal{Y}_D^T \mathcal{Y}_e^* \mathcal{Y}_e^T \mathcal{Y}_D^* \right) + \dots \right] \quad (34)$$

where, for clarity, only the terms not flavour aligned have been written explicitly. (The additional terms in eq. (34) will be fully written out later on.) Due to the inclusion of \mathcal{Y}_e , $\delta\mu_N$ cannot be diagonalised by the same orthogonal matrix \mathcal{O} , since $\mathcal{Y}_e \mathcal{Y}_e^\dagger \not\propto \text{Re} \{ \mathcal{Y}_D^\dagger \mathcal{Y}_D \}$. Changing to the mass basis now allows off-diagonal real terms and therefore the generation of a non-zero asymmetry. The necessary off-diagonal entries, however, are generated by the misalignment between the two spurions, and thus they will be suppressed compared to if they had been generated at leading order.

Due to the extra fields introduced, the above flavour alignment problem does not occur in general for the extended seesaw models. Consider the full ISS + LSS scenario where the equivalent radiative corrections to the relevant Majorana masses are included,

$$\begin{pmatrix} 0 & m_D & m_L \\ m_D^T & \mu_N \mathbb{1}_3 + \delta\mu_N & m_R \mathbb{1}_3 \\ m_L^T & m_R \mathbb{1}_3 & \mu_S \mathbb{1}_3 + \delta\mu_S \end{pmatrix} \rightarrow \begin{pmatrix} 0 & m_D \mathcal{O} & m_L \mathcal{V} \\ \mathcal{O}^T m_D^T & \hat{\mu}_N & m_R \mathcal{V} \mathcal{O}^T \\ \mathcal{V}^T m_L^T & m_R \mathcal{V}^T \mathcal{O} & \hat{\mu}_S \end{pmatrix}. \quad (35)$$

Here $\hat{\mu}_i = \text{diag}(\dots)$ and the rotation matrices \mathcal{O} and \mathcal{V} diagonalise $\delta\mu_N$ and $\delta\mu_S$ respectively. The spoiling of the flavour alignment should be clear: in the process of diagonalising the Majorana mass terms μ_i , the Dirac mass between the two heavy SNs $m_R \mathbb{1}_3$ has been rotated as well. Diagonalising the lower right 2×2 block will now no longer rotate the Dirac mass matrices m_D and m_L by the same orthogonal rotation that diagonalises $\mathcal{Y}_D^\dagger \mathcal{Y}_D$. The same alignment effect can occur only for very specific choices between the entries of eq. (35) and is not a general feature. We will provide an illustrative example below.

A. Baryon Asymmetry

In this section we briefly describe the procedure and formalism we employ for estimating the efficiency of asymmetry generation. A more detailed explanation of our conventions, definitions and numerical calculations can be found in [43]. These, in turn, are based on the Boltzmann equations (BEs) derived in [21, 22] specifically for flavoured leptogenesis in the resonant regime.

As is conventional, we work in the heavy sterile neutrino mass basis, i.e. the bottom-right sub-matrix of Eq. (20) is real, positive and diagonal. The block diagonalisation of the lower right 2×2 block defines the rotation,

$$M_\nu \rightarrow U_{\text{rot}}^T M_\nu U_{\text{rot}} \equiv M'_\nu = \begin{pmatrix} m_\nu^{\text{loop}} & m'_D & m'_L \\ (m'_D)^T & \hat{M}_+ & 0 \\ (m'_L)^T & 0 & \hat{M}_- \end{pmatrix}, \quad (36)$$

where primed parameters indicate rotated matrices and $\hat{M}_i = \text{diag}(\dots)$. We have included the one-loop contribution to the active neutrino masses which may significantly contribute in some regions of parameter space. In the most general case, a simple analytic expression for the rotated matrices m'_i is not possible. However, in our setup, where an $SO(3)^2$ flavour symmetry is employed (and before radiative effects are included) the entries of the bottom-right 2×2 sub-block are all commuting. Under this simplification the rotation can be generalised from the simple one-generation case, giving

$$U_{\text{rot}} = \begin{pmatrix} \mathbb{1}_3 & & & 0 \\ 0 & \cos \left[\frac{\pi}{4} + \frac{1}{2} \arctan \left(\frac{\mu_S - \mu_N}{2m_R} \right) \right] \mathbb{1}_3 & -i \sin \left[\frac{\pi}{4} + \frac{1}{2} \arctan \left(\frac{\mu_S - \mu_N}{2m_R} \right) \right] \mathbb{1}_3 \\ 0 & \sin \left[\frac{\pi}{4} + \frac{1}{2} \arctan \left(\frac{\mu_S - \mu_N}{2m_R} \right) \right] \mathbb{1}_3 & i \cos \left[\frac{\pi}{4} + \frac{1}{2} \arctan \left(\frac{\mu_S - \mu_N}{2m_R} \right) \right] \mathbb{1}_3 \end{pmatrix} \quad (37)$$

leading to

$$\begin{aligned} m'_D &= \cos \left[\frac{1}{4} \left(\pi + 2 \arccot \left[\frac{2m_R}{\mu_S - \mu_N} \right] \right) \right] m_D + \sin \left[\frac{1}{4} \left(\pi + 2 \arccot \left[\frac{2m_R}{\mu_S - \mu_N} \right] \right) \right] m_L \\ &\simeq \left(\frac{1}{\sqrt{2}} - \frac{1}{4\sqrt{2}} \left(\frac{\mu_S - \mu_N}{2m_R} \right) \right) m_D + \left(\frac{1}{\sqrt{2}} + \frac{1}{4\sqrt{2}} \left(\frac{\mu_S - \mu_N}{2m_R} \right) \right) m_L \\ m'_L &= -i \sin \left[\frac{1}{4} \left(\pi + 2 \arccot \left(\frac{2m_R}{\mu_S - \mu_N} \right) \right) \right] m_D + i \cos \left[\frac{1}{4} \left(\pi + 2 \arccot \left(\frac{2m_R}{\mu_S - \mu_N} \right) \right) \right] m_L \end{aligned}$$

$$\begin{aligned}
&\simeq -i \left(\frac{1}{\sqrt{2}} + \frac{1}{4\sqrt{2}} \left(\frac{\mu_S - \mu_N}{2m_R} \right) \right) m_D + i \left(\frac{1}{\sqrt{2}} - \frac{1}{4\sqrt{2}} \left(\frac{\mu_S - \mu_N}{2m_R} \right) \right) m_L \\
\hat{M}_+ &= \left(m_R \sqrt{1 + \frac{(\mu_S - \mu_N)^2}{4m_R^2}} + \frac{\mu_S}{2} + \frac{\mu_N}{2} \right) \mathbb{1}_3 \\
&\simeq \left(m_R + \frac{\mu_S}{2} + \frac{\mu_N}{2} \right) \mathbb{1}_3 \\
\hat{M}_- &= \left(m_R \sqrt{1 + \frac{(\mu_S - \mu_N)^2}{4m_R^2}} - \frac{\mu_S}{2} - \frac{\mu_N}{2} \right) \mathbb{1}_3 \\
&\simeq \left(m_R - \frac{\mu_S}{2} - \frac{\mu_N}{2} \right) \mathbb{1}_3
\end{aligned} \tag{38}$$

where in every second line we have expanded up to $\mathcal{O}(\frac{\mu_S - \mu_N}{m_R})$. Once the spurionic radiative corrections are included in the Majorana self-energies, the $\mathcal{O}(3)^2$ invariance is lifted and the matrices no longer commute. In the regime where these corrections are small these expressions will remain approximately valid. However, once the corrections are included, we perform the rotations numerically during our scan.

The combination

$$h^\dagger h \simeq \frac{2}{v^2} \begin{pmatrix} m_D'^\dagger m_D' & m_D'^\dagger m_L' \\ m_L'^\dagger m_D' & m_L'^\dagger m_L' \end{pmatrix} \tag{39}$$

where $h = \frac{\sqrt{2}}{v} (m_D', m_L')$, is now the relevant combination for flavoured leptogenesis. The entries in the diagonal blocks of $h^\dagger h$ control the CP asymmetry generated between two different generations of heavy SNs with same sign mass splitting

$$\Delta m_{i,j}^{\text{SS}} = (\hat{M}_\pm)_{ii} - (\hat{M}_\pm)_{jj}. \tag{40}$$

The off-diagonal blocks control the CP asymmetry generated between heavy SNs of opposite mass splitting (same generation or otherwise)

$$\Delta m_{i,j}^{\text{OS}} = (\hat{M}_\pm)_{ii} - (\hat{M}_\mp)_{jj}. \tag{41}$$

Clearly, in the absence of radiative effects where we have $\mu_N, \mu_S \propto \mathbb{1}_3$ only $\Delta m_{i,j}^{\text{OS}} \neq 0$, with $\Delta m_{i,j}^{\text{SS}} = 0$. Once the corrections are included, however, the $SO(3)^2$ invariance is broken allowing for both $\Delta m_{i,j}^{\text{OS}} \neq 0$ and $\Delta m_{i,j}^{\text{SS}} \neq 0$. From eqs. (38) and (39) it can be seen that for example if $m_D = m_L$ ¹⁰ along with $\mu_N = \mu_S$ then $m_D' \neq 0$ but $m_L' = 0$. No real, off-diagonal entries would exist and the same alignment problem of the type-I seesaw would

¹⁰ This would imply that $\delta\mu_N = \delta\mu_S$ and therefore $\mathcal{O} = \mathcal{V}$.

occur. This is not a general feature in the extended MLFV seesaw (as it is in the minimal type-I MLFV seesaw) and would require an additional symmetry to enforce the necessary relations between the couplings and masses such that this flavour alignment would occur.

We consider a low-scale scenario in which the sterile masses are set to $\mathcal{O}(\text{TeV})$. This implies a low-temperature regime of lepton asymmetry generation where individual lepton flavours are in equilibrium with the thermal bath and distinguishable. We employ *flavour-dependent* Boltzmann equations [22, 79] for which we define the CP asymmetry generated from the decays of an SN, N_i , to a specific lepton flavour ℓ_α ,

$$\varepsilon_\alpha^i = \frac{\Gamma(N_i \rightarrow l_\alpha \Phi) - \Gamma(N_i \rightarrow (l_\alpha)^c \Phi^\dagger)}{\sum_\alpha [\Gamma(N_i \rightarrow l_\alpha \Phi) + \Gamma(N_i \rightarrow (l_\alpha)^c \Phi^\dagger)]}. \quad (42)$$

These have been calculated previously [21, 22] for the general case relevant for both hierarchical and degenerate scenarios with potential resonance effects [80] included. The result, separated into vertex ε_V and self-energy ε_S contributions, is

$$\varepsilon_i^\alpha = \frac{1}{8\pi (h^\dagger h)_{ii}} \sum_{j \neq i} \left(\underbrace{\mathcal{A}_{ij}^\alpha f(x_{ij})}_{\varepsilon_V} + \underbrace{(\mathcal{A}_{ij}^\alpha \sqrt{x_{ij}} + \mathcal{B}_{ij}^\alpha) \frac{\sqrt{x_{ij}} (1 - x_{ij})}{(1 - x_{ij})^2 + \frac{1}{64\pi^2} (h^\dagger h)_{jj}^2}}_{\varepsilon_S} \right) + \mathcal{O}(h^6) \dots \quad (43)$$

where $\mathcal{A}_{ij}^\alpha = \text{Im} \left\{ (h^\dagger h)_{ij} h_{\alpha i}^* h_{\alpha j} \right\}$, $\mathcal{B}_{ij}^\alpha = \text{Im} \left\{ (h^\dagger h)_{ji} h_{\alpha i}^* h_{\alpha j} \right\}$, $x_{ij} = \left(\frac{m_{N_j}}{m_{N_i}} \right)^2$ and the loop function for the vertex-diagram contribution $f(x_{ij})$, is given by [6]

$$f(x_{ij}) = \sqrt{x_{ij}} \left[1 - (1 + x_{ij}) \ln \left(\frac{1 + x_{ij}}{x_{ij}} \right) \right]. \quad (44)$$

A resonant enhancement in the CP asymmetry will occur when

$$1 - x_{ij} \rightarrow \frac{1}{8\pi} (h^\dagger h)_{jj} \quad (45)$$

which leads to the simplified condition

$$m_{N_i} - m_{N_j} \rightarrow \frac{\Gamma_{i,j}}{2} \quad (46)$$

where $\Gamma_i \simeq \frac{m_i}{8\pi} \sum_l h_{li}^* h_{li}$ is the decay width of N_i and we assume $m_{N_i} - m_{N_j} \ll m_{N_{i,j}}$ in order to move from eq. (45) to (46).

We choose the regulator of ε_α^i to be of the form $m_i \Gamma_j$, which as discussed in Appendix A of [55] has consistent behaviour for models with approximate lepton-number conservation.

For other choices of regulators unphysical behaviour may be encountered in such a scenario. For example choosing a regulator of the form $(m_i\Gamma_i - m_j\Gamma_j)$ diverges in the scenario $m_i \rightarrow m_j$ combined with $\Gamma_i \rightarrow \Gamma_j$ which occurs as the LNV parameters are taken to zero.

Specifically for the LSS scenario, it is important to note that the second term in eq. (43), due to the one-loop *self-energy* correction ε_S , identically goes to zero when $m_{N_i} \rightarrow m_{N_j}$. By contrast, the first term arises from the one-loop *vertex* correction ε_V . In the limit $m_{N_i} \rightarrow m_{N_j}$ the asymmetry it generates is non-zero. However, $A_{ij}^\alpha = -A_{ji}^\alpha$ and therefore

$$\varepsilon_i^\alpha = -\frac{(h^\dagger h)_{ii}}{(h^\dagger h)_{jj}} \varepsilon_j^\alpha \quad (47)$$

for $m_{N_i} = m_{N_j}$. Therefore the asymmetry produced by the decay of N_i to flavour α is almost equal and opposite to that of N_j and in the limit $(h^\dagger h)_{ii} \rightarrow (h^\dagger h)_{jj}$ the asymmetry will vanish identically once the decays of all SNs are included. If the two SNs have different decay widths a non-zero asymmetry is possible, albeit highly suppressed.

We will work under the condition that, due to the strong washout nature of the temperature regime we favour [43], asymmetry generation occurs predominately well before the electroweak phase transition crossover and so we need not consider the changing sphaleron rate as the temperature approaches and crosses its critical value. The baryon asymmetry is then expressed as a fraction of the lepton asymmetry generated through

$$\eta_B = -\frac{28}{51} \frac{1}{27} \sum_{\alpha=e,\mu,\tau} \eta_\alpha \quad (48)$$

where the factor of 28/51 arises from the fraction of lepton asymmetry reprocessed into a baryon asymmetry by electroweak sphalerons [81], while the dilution factor 1/27 arises from photon production until the recombination epoch [82].

IV. NUMERICAL RESULTS

In full analogy to the type-I scenario, all appropriate flavour invariant operators must be included. This leads to corrections to the Majorana mass terms from spurion combinations transforming the appropriate way such that when coupled with the heavy SN fields, the term is flavour invariant at the high scale. Now in the case of the extended seesaw both

Majorana masses receive corrections, as per

$$\begin{aligned}\tilde{\mu}_N &= \mu_N \left(\mathcal{Y}_{\mu_N} + n_1 \left(\mathcal{Y}_D^\dagger \mathcal{Y}_D + (\mathcal{Y}_D^\dagger \mathcal{Y}_D)^T \right) + n_2^{(1)} \left(\mathcal{Y}_D^\dagger \mathcal{Y}_D \mathcal{Y}_D^\dagger \mathcal{Y}_D + (\mathcal{Y}_D^\dagger \mathcal{Y}_D \mathcal{Y}_D^\dagger \mathcal{Y}_D)^T \right) + \dots \right) \\ \tilde{\mu}_S &= \mu_S \left(\mathcal{Y}_{\mu_S} + s_1 \left(\mathcal{Y}_L^\dagger \mathcal{Y}_L + (\mathcal{Y}_L^\dagger \mathcal{Y}_L)^T \right) + s_2^{(1)} \left(\mathcal{Y}_L^\dagger \mathcal{Y}_L \mathcal{Y}_L^\dagger \mathcal{Y}_L + (\mathcal{Y}_L^\dagger \mathcal{Y}_L \mathcal{Y}_L^\dagger \mathcal{Y}_L)^T \right) + \dots \right).\end{aligned}\tag{49}$$

As can be checked explicitly by applying the transformations defined in eq. (25), the combinations of spurions above are flavour invariant when coupled to $\overline{N}_R^c N_R$ and $\overline{S}_L^c S_L$. All terms at next-to-leading order in the flavour-invariant spurion insertions will be explicitly written below.

The coefficients n_i and s_i are dimensionless Wilson coefficients which are treated as free parameters in the absence of an explicit high-scale, renormalisable theory. They are conventionally either taken to be $\mathcal{O}(1)$ numbers [46, 47, 52, 83], or arising from radiative effects [53, 54] so that $n_1 \simeq s_1 \simeq \frac{1}{16\pi^2}$ and $s_2^{(i)} \sim (s_1)^2$ etc. Note that in the ISS regime where $\mathcal{Y}_L = 0$, only the Majorana mass μ_N receives radiative corrections from flavour effects in our setup, whereas in the LSS regime where $\mathcal{Y}_{\mu_N} = \mathcal{Y}_{\mu_S} = 0$ both Majorana masses receive corrections.

We consider the general scenario where one copy of N_R and S_L is added for each generation of active neutrino. The tree-level light neutrino mass matrix can be expressed in powers of the LNV parameters [84] which in complete generality (without assuming MLFV) can be expanded to

$$\begin{aligned}m_\nu^{\text{tree}} = & m_D \left(M_R^T \right)^{-1} \mu_S M_R^{-1} m_D^T + m_D \left(M_R^T \right)^{-1} \mu_S M_R^{-1} \mu_N \left(M_R^T \right)^{-1} \mu_S M_R^{-1} m_D^T \\ & - m_L M_R^{-1} m_D^T - m_L M_R^{-1} \mu_N \left(M_R^T \right)^{-1} \mu_S M_R^{-1} m_D^T \\ & - m_D \left(M_R^T \right)^{-1} m_L^T - m_D \left(M_R^T \right)^{-1} \mu_S M_R^{-1} \mu_N \left(M_R^T \right)^{-1} m_L^T \\ & + m_L M_R^{-1} \mu_N \left(M_R^T \right)^{-1} m_L^T + m_L M_R^{-1} \mu_N \left(M_R^T \right)^{-1} \mu_S M_R^{-1} \mu_N \left(M_R^T \right)^{-1} m_L^T \\ & + \dots\end{aligned}\tag{50}$$

where for completeness we have written all leading and next-to-leading terms valid for $\|\mu_S\|, \|\mu_N\|, \|m_L\| \ll \|M_R\|$. The above equation is valid for the general case of non-commuting sub-matrices, but for our MLFV setup $M_R = m_R \mathbb{1}_3$, m_L is diagonal and $\mu_S \propto \mu_N \propto \mathbb{1}_3$.

In the limiting case of the ISS, only the first line of eq. (50) contributes at leading order to the active neutrino masses. This mass vanishes in the limit $\mu_S \rightarrow 0$ even if $\mu_N \neq 0$. Even for $\mu_S \neq 0$ the contribution from μ_N is highly suppressed, including for a large regime where $\mu_N \gg \mu_S$.

At one-loop order, additional terms are generated for the active neutrino masses which can be important [84],

$$m_\nu^{\text{loop}} \simeq \frac{f(m_R)}{m_W^2} \left(m_D \mu_N m_D^T + m_L \mu_S m_L^T + m_R m_L m_D^T + m_R m_D m_L^T \right) \quad (51)$$

where

$$f(x) = \frac{\alpha_W}{16\pi} \left(\frac{m_H^2}{x^2 - m_H^2} \ln \left[\frac{x^2}{m_H^2} \right] + \frac{3m_Z^2}{x^2 - m_Z^2} \ln \left[\frac{x^2}{m_Z^2} \right] \right) \quad (52)$$

is a one-loop function and eq. (51) is only valid for $M_R = m_R \mathbb{1}_3$. Different terms in eq. (51) can contribute significantly for different hierarchies amongst μ_N , μ_S and m_L which are free parameters in our scan.

Combining the tree-level and one-loop contribution at leading order leads to a general light-neutrino mass matrix in our MLFV Ansatz of the form

$$m_\nu = \underbrace{\frac{1}{m_R^2} \left(f(m_R) \frac{m_R^2}{m_W^2} \right) \left(m_D \mu_N m_D^T + m_L \mu_S m_L^T \right) + \frac{1}{m_R} \left(f(m_R) \frac{m_R^2}{m_W^2} \right) (m_L m_D^T + m_D m_L^T)}_{\text{one-loop}} + \underbrace{\frac{1}{m_R^2} \left(m_D \mu_N m_D^T + m_L \mu_S m_L^T \right) - \frac{1}{m_R} (m_L m_D^T + m_D m_L^T)}_{\text{tree}}. \quad (53)$$

For both the ISS and LSS we fix $m_R = 1$ TeV. For the ISS specifically, the LNV parameters are randomly (and independently) scanned over the ranges

$$\begin{aligned} \mu_S &\sim \mathcal{O}(10^{-15} - 10^2) \mathbb{1}_3 \text{ GeV} \\ \mu_N &\sim \mathcal{O}(10^{-15} - 10^4) \mathbb{1}_3 \text{ GeV} \end{aligned} \quad (54)$$

where we allow for larger values of μ_N over μ_S as its contribution to the active neutrino mass is suppressed by a loop factor. For the LSS we vary

$$(m_L)_{ii} \sim \mathcal{O}(10^{-9} - 10^1) \text{ GeV} \quad (55)$$

where, in order to reduce the number of degrees of freedom, we take it to be diagonal but not proportional to the identity matrix in order for its inclusion to break the flavour symmetry.

We fit active-neutrino data by fixing the Dirac mass matrix m_D with an *approximate*¹¹ Casas-Ibarra parameterisation [85] which for the ISS is

$$m_D = m_R U_{\text{PMNS}} \hat{m}_\nu^{1/2} R \mu_{\text{eff}}^{-1/2}, \quad (56)$$

where we define an effective mass

$$\mu_{\text{eff}} = f(m_R) \left(\frac{m_R}{m_W} \right)^2 \mu_N + \mu_S. \quad (57)$$

For the LSS,

$$m_D = -m_R U \hat{m}_\nu^{1/2} C \hat{m}_\nu^{1/2} U_{\text{PMNS}}^T (m_L^{\text{eff}})^{T-1} \quad (58)$$

with an equivalently defined effective mass

$$m_L^{\text{eff}} = \left(f(m_R) \left(\frac{m_R}{m_W} \right)^2 - 1 \right) m_L. \quad (59)$$

The matrix R is a complex-orthogonal matrix $R R^T = \mathbb{1}_3$ which can be parameterised with three complex mixing angles $\theta_i = \theta_i^r + i\theta_i^c$ where

$$R(\theta_1, \theta_2, \theta_3) = R_{12}(\theta_1) R_{13}(\theta_2) R_{23}(\theta_3),$$

$$R_{12}(\theta_1) = \begin{pmatrix} \cos \theta_1 & -\sin \theta_1 & 0 \\ \sin \theta_1 & \cos \theta_1 & 0 \\ 0 & 0 & 1 \end{pmatrix}, \quad R_{13}(\theta_2) = \begin{pmatrix} \cos \theta_2 & 0 & -\sin \theta_2 \\ 0 & 1 & 0 \\ \sin \theta_2 & 0 & \cos \theta_2 \end{pmatrix}, \quad R_{23}(\theta_3) = \begin{pmatrix} 1 & 0 & 0 \\ 0 & \cos \theta_3 & -\sin \theta_3 \\ 0 & \sin \theta_3 & \cos \theta_3 \end{pmatrix} \quad (60)$$

and we have defined $\cos(x) \equiv \cos_x$ and $\sin(x) \equiv \sin_x$ in the usual way.

In order to reduce the number of free parameters we fix the real components of the mixing angles to

$$\theta_1^r = \frac{\pi}{5}, \quad \theta_2^r = \frac{5\pi}{6}, \quad \theta_3^r = \frac{4\pi}{7} \quad (61)$$

where there is no significance to the values chosen. The asymmetry is not sensitive to the values of the real angles [43] and therefore should apply for any choice of their values. We fix $\theta_1^c = \theta_3^c = 0$ for simplicity and scan over

$$\theta_2^c \sim \mathcal{O}(10^{-3} - 10^1). \quad (62)$$

¹¹ The parameterisation is only approximate as we ignore the corrections to the mass terms e.g. $\tilde{\mu}_i = \mu_i + \delta\mu_i$ generated through spurion insertions when solving for m_D . This approximation is valid in the regime where $\delta\mu_i < \mu_i$. We additionally check that once these corrections are included the active-neutrino mass differences are not spoiled.

By contrast to the complex-orthogonal R , the matrix C instead satisfies $C + C^T = \mathbb{1}_3$ and therefore must be an anti-symmetric matrix of the specific form,

$$C = \begin{pmatrix} \frac{1}{2} & a_1 & a_2 \\ -a_1 & \frac{1}{2} & a_3 \\ -a_2 & -a_3 & \frac{1}{2} \end{pmatrix} \quad (63)$$

with $a_i = a_i^r + ia_i^c$ where we choose to fix

$$a_1^r = \frac{1}{10}, \quad a_2^r = \frac{2}{10}, \quad a_3^r = \frac{1}{2}, \quad a_1^c = a_3^c = 0 \quad (64)$$

and scan over

$$a_2^c \sim \mathcal{O}(10^{-3} - 10^1). \quad (65)$$

The active-neutrino masses

$$\hat{m}_\nu = \text{diag}(m_{\nu_1}, m_{\nu_2}, m_{\nu_3}) = U_{\text{PMNS}}^\dagger (m_\nu^{\text{tree}} + m_\nu^{\text{loop}}) U_{\text{PMNS}}^* \quad (66)$$

are inputs for eqs. (56) and (58) where for simplicity we assume normal ordering which is currently favoured over inverted ordering [74], implying

$$\begin{aligned} m_{\nu_2} &= \sqrt{m_{\nu_1}^2 + \Delta m_{21}^2} \\ m_{\nu_3} &= \sqrt{m_{\nu_1}^2 + \Delta m_{21}^2 + \Delta m_{31}^2} \end{aligned} \quad (67)$$

and unless stated otherwise we fix the lightest neutrino mass m_{ν_1} to 0.01 eV. Other active neutrino parameters are fixed to their current best fit values [74] and listed in table V, while the Dirac phase has been fixed to be maximally CP-violating.

We work in the perturbative regime of the Yukawa couplings generated by the Casas-Ibarra parameterisations such that $|\mathcal{Y}_{ij}|^2 \lesssim 4\pi$, which prevents very large choices for the complex parameters. We fix the unknown Wilson coefficients s_i and n_i to $\frac{1}{16\pi^2}$ for definiteness unless stated otherwise.

To check our numerical solutions to the Boltzmann equations, we compare the results to a known approximate analytic expression of the baryon asymmetry that is valid in the strong washout regime ($K_{\text{eff}}^\alpha \geq 5$) [82, 86], where

Parameter	Value
$\sin^2 \theta_{12}$	0.310
$\sin^2 \theta_{23}$	0.580
$\sin^2 \theta_{13}$	0.02241
$\Delta m_{21}^2 / (10^{-5} \text{ eV}^2)$	$7.39^{+0.19}_{-0.17}$
$\Delta m_{31}^2 / (10^{-3} \text{ eV}^2)$	$2.525^{+0.039}_{-0.040}$
δ_{CP}	$3\pi/2$

TABLE V: List of experimental measurements of the parameters in the PMNS matrix and the light neutrino mass splittings fixed by active neutrino oscillation experiments. The light neutrino mass differences were allowed to vary within 1σ of their current best fit values [74].

$$K_\alpha^{\text{eff}} = \kappa^\alpha \sum_i K_i J_i^\alpha, \quad (68)$$

$$\kappa^\alpha = 2 \sum_{i,j(j \neq i)} \frac{\text{Re}[(h)_{i\alpha}(h)_{j\alpha}^* (hh^\dagger)_{ij}] + \text{Im}[(h)_{i\alpha}(h)_{j\alpha}^*]^2}{\text{Re}[(h^\dagger h)_{\alpha\alpha} \{ (hh^\dagger)_{ii} + (hh^\dagger)_{jj} \}]} \left(1 - 2i \frac{m_{N_i} - m_{N_j}}{\Gamma_i + \Gamma_j}\right)^{-1}, \quad (69)$$

$$J_i^\alpha = \frac{\Gamma(N_i \rightarrow l_\alpha \Phi) + \Gamma(N_i \rightarrow l_\alpha^c \Phi^\dagger)}{\sum_\alpha [\Gamma(N_i \rightarrow (l_\alpha)^c \Phi) + \Gamma(N_i \rightarrow (l_\alpha)^c \Phi^\dagger)]}, \quad (70)$$

with $m_{N_i} = (\hat{M}_\pm)_{ii}$. The asymmetry is approximated by

$$\eta_B^{\text{approx.}} = -\frac{28}{51} \frac{1}{27} \frac{3}{2} \sum_{\alpha,i} \frac{\varepsilon_i^\alpha}{K_{\text{eff}}^\alpha \text{Min}[z_c, 1.25 \ln(25 K_{\text{eff}}^\alpha)]}. \quad (71)$$

The numerical versus analytic approximation comparison illustrated in table VI provides strong evidence that our numerical routines are accurate.

Example parameters	$ \eta_B $	$ \eta_B^{\text{approx.}} $
$m_L \simeq \text{diag}(1.5, 2.6, 1.2) \times 10^{-3} \text{ GeV}$		
$\mu_S = \mu_N = 0$	1.37×10^{-10}	7.23×10^{-10}
$a_1 = \frac{1}{10}, \quad a_2 \simeq \frac{2}{10} + 0.00028i, \quad a_3 = \frac{5}{10}$		
$m_L \simeq \text{diag}(0.70, 1.33, 1.26) \times 10^{-5} \text{ GeV}$		
$\mu_S = \mu_N = 0$	1.98×10^{-11}	2.31×10^{-11}
$a_1 = \frac{1}{10}, \quad a_2 \simeq \frac{2}{10} + 2.06i, \quad a_3 = \frac{5}{10}$		
$m_L = 0$		
$\mu_S \simeq 9 \times 10^{-11} \text{ GeV}, \quad \mu_N \simeq 225 \text{ GeV}$	2.57×10^{-11}	1.21×10^{-11}
$\theta_1 = \frac{\pi}{5}, \quad \theta_2 \simeq \frac{5\pi}{6} + 0.094i, \quad \theta_3 = \frac{4\pi}{7}$		
$m_L = 0$		
$\mu_S \simeq 1 \text{ GeV}, \quad \mu_N \simeq 414 \text{ GeV}$	1.71×10^{-10}	5.75×10^{-11}
$\theta_1 = \frac{\pi}{5}, \quad \theta_2 \simeq \frac{5\pi}{6} + 0.16i, \quad \theta_3 = \frac{4\pi}{7}$		

TABLE VI: Comparison between the numerically computed asymmetry $|\eta_B|$ and the analytic approximation $|\eta_B^{\text{approx.}}|$ from eq. (71) for example points of the LSS (top two) and ISS (bottom two). All points include all relevant radiative corrections as defined in eq. (49) where for these example parameters we have set all Wilson coefficients at lowest order to

$$1/16\pi^2.$$

A. Inverse seesaw (ISS)

For the ISS ($\mathcal{Y}_L = 0$,) the only LNV parameters present are the two small Majorana masses

$$M_\nu = \begin{pmatrix} m_\nu^{\text{loop}} & m_D & 0 \\ m_D^T & \mu_N & M_R \\ 0 & M_R^T & \mu_S \end{pmatrix}. \quad (72)$$

From eq. (49) only μ_N receives radiative corrections from $SO(3)_{N_R}$ breaking terms proportional to the Yukawa spurion \mathcal{Y}_D .

We separately consider three scenarios for the ISS: first where no corrections are intro-

duced, second where corrections are introduced at the next lowest order, labelled \mathcal{N}_1 and, third, corrections up to next-to-leading order, labelled \mathcal{N}_2 :

$$\tilde{\mu}_N = \mu_N \left(\mathbb{1}_3 + \mathcal{N}_1 + \mathcal{N}_2 \right) \quad (73)$$

where

$$\begin{aligned} \mathcal{N}_1 &= n_1 \left(\mathcal{Y}_D^\dagger \mathcal{Y}_D + (\mathcal{Y}_D^\dagger \mathcal{Y}_D)^T \right), \\ \mathcal{N}_2 &= n_2^{(1)} \left(\mathcal{Y}_D^\dagger \mathcal{Y}_D \mathcal{Y}_D^\dagger \mathcal{Y}_D + (\mathcal{Y}_D^\dagger \mathcal{Y}_D \mathcal{Y}_D^\dagger \mathcal{Y}_D)^T \right) + n_2^{(2)} \left(\mathcal{Y}_D^\dagger \mathcal{Y}_D (\mathcal{Y}_D^\dagger \mathcal{Y}_D)^T \right) \\ &\quad + n_2^{(3)} \left((\mathcal{Y}_D^\dagger \mathcal{Y}_D)^T \mathcal{Y}_D^\dagger \mathcal{Y}_D \right) + n_2^{(4)} \left(\mathcal{Y}_D^\dagger \mathcal{Y}_e \mathcal{Y}_e^\dagger \mathcal{Y}_D + (\mathcal{Y}_D^\dagger \mathcal{Y}_e \mathcal{Y}_e^\dagger \mathcal{Y}_D)^T \right) \end{aligned} \quad (74)$$

and we fix $n_2^{(i)} = (n_1)^2$ for computational convenience. Due to the perturbative regime in which we operate, it will always be the case that $\|\mathcal{N}_i\| \ll 1$. All terms are formally flavour invariant and serve to break the flavour degeneracy amongst the heavy SNs when these spurions acquire non-zero VEVs.

For the ISS as $m_L = 0$ the combination in eq. (39) simplifies to

$$h^\dagger h \simeq \frac{2}{v^2} \begin{pmatrix} \left(\frac{1}{\sqrt{2}} - \frac{1}{4\sqrt{2}} \left(\frac{\mu_S - \mu_N}{2m_R} \right) \right)^2 m_D^\dagger m_D & -i \left(\frac{1}{2} - \frac{1}{32} \left(\frac{\mu_S - \mu_N}{2m_R} \right)^2 \right) m_D^\dagger m_D \\ i \left(\frac{1}{2} - \frac{1}{32} \left(\frac{\mu_S - \mu_N}{2m_R} \right)^2 \right) m_D^\dagger m_D & \left(\frac{1}{\sqrt{2}} + \frac{1}{4\sqrt{2}} \left(\frac{\mu_S - \mu_N}{2m_R} \right) \right)^2 m_D^\dagger m_D \end{pmatrix} \quad (75)$$

where we are now dealing with unprimed matrices. Due to the fact that $M_R \propto \mu_S \propto \mathbb{1}_3$, in the case where only \mathcal{N}_1 is included the corrected Majorana mass μ_N can be diagonalised without affecting the other entries in the 2×2 sub-block, with

$$\begin{pmatrix} 0 & m_D & 0 \\ m_D^T & \mu_N \mathbb{1}_3 + \delta\mu_N & m_R \mathbb{1}_3 \\ 0 & m_R \mathbb{1}_3 & \mu_S \mathbb{1}_3 \end{pmatrix} \rightarrow \begin{pmatrix} 0 & m_D \mathcal{O} & 0 \\ \mathcal{O}^T m_D^T & \hat{\mu}_N & m_R \mathbb{1}_3 \\ 0 & m_R \mathbb{1}_3 & \mu_S \end{pmatrix} \quad (76)$$

under the rotation $N_R \rightarrow \mathcal{O} N_R$ and $S_L \rightarrow \mathcal{O} S_L$. *Similarly* to the minimal type-I scenario, if only \mathcal{N}_1 is included then $\text{Re} \{ m_D^\dagger m_D \} \propto \mathcal{N}_1 = \delta\mu_N$ and the combinations of $m_D^\dagger m_D$ appearing in eq. (75) will have no real off-diagonal components. We emphasize that this only occurs for the ISS because $m_L = 0$. *Differently* to the type-I scenario however the off-diagonal blocks of eq. (75) have an additional complex phase such that the imaginary

components¹² of $\mathcal{O}^T m_D^\dagger m_D \mathcal{O}$ become real off-diagonal entries in $h^\dagger h$. This therefore allows for non-zero generation of lepton asymmetry unlike the type-I scenario.

As only the off-diagonal blocks of $h^\dagger h$ contain the necessary terms, only diagrams between two SNs of different mass splittings, i.e. from $\Delta m_{i,j}^{\text{OS}}$, will contribute to asymmetry. The real components of the (1, 1) and (2, 2) blocks are diagonal, on the other hand, meaning that SNs with the same sign mass splitting $\Delta m_{i,j}^{\text{SS}}$ will not contribute to ε_α^i . Once \mathcal{N}_2 is included however, the flavour mis-alignment between $\delta\mu_N$ and $m_D^\dagger m_D$ will generate real off-diagonal components in $m_D^\dagger m_D$ and therefore all four blocks of eq. (75) will contribute to ε_α^i .

In fig. 1 we plot the baryon asymmetry numerically calculated as a function of both μ_N and μ_S . All three scenarios are simultaneously plotted. Both in the case where radiative effects are ignored as well as when only \mathcal{N}_1 is included, similar behaviour occurs. The inclusion of \mathcal{N}_1 breaks the mass degeneracy between all six SNs, as opposed to without its inclusion where two groups of identical mass SNs form. However, as discussed above, due to flavour alignment only diagrams involving opposite mass split SNs contribute to the asymmetry. Therefore the mass difference is generated exclusively from

$$\Delta m_{i,j}^{\text{OS}} = (m_{N_\pm})_i - (m_{N_\mp})_j \simeq \mu_N + \mu_S \quad (77)$$

with

$$m_{N_\pm} \simeq m_R \pm \frac{1}{2}\mu_N \pm \frac{1}{2}\mu_S. \quad (78)$$

While the spurion corrections are present we have $\mu_N \gg \mathcal{N}_1$ and therefore they are not the dominant source for the mass splittings in this situation. In this regime resonant leptogenesis is not feasible [43–45]. The inclusion of \mathcal{N}_2 generates non-zero, off-diagonal entries in the (1, 1) and (2, 2) entries of eq. (75) such that new contributions turn on arising from the mass splitting

$$\Delta m_{i,j}^{\text{SS}} = (m_{N_\pm})_i - (m_{N_\pm})_j \simeq \mu_N (\mathcal{Y}_D^\dagger \mathcal{Y}_D)_{ii}. \quad (79)$$

We emphasize that even when only \mathcal{N}_1 is included, the mass degeneracy between the same sign mass split SNs is still broken $\Delta m_{i,j}^{\text{SS}} \neq 0$. No resonant enhancement occurs between two such SNs in this case not because of a mass degeneracy between them (as is the case when no corrections are included) but because of the flavour alignment issue described above.

¹² This is because $\mathcal{O}^T \text{Re} \left\{ \mathcal{Y}_D^\dagger \mathcal{Y}_D \right\} \mathcal{O} = \text{diag}(\dots)$ due to the form of the corrections but $\mathcal{O}^T \text{Im} \left\{ \mathcal{Y}_D^\dagger \mathcal{Y}_D \right\} \mathcal{O} \neq \text{diag}(\dots)$ and therefore off-diagonal imaginary components are generated which become real due to the additional phase in eq. (75).

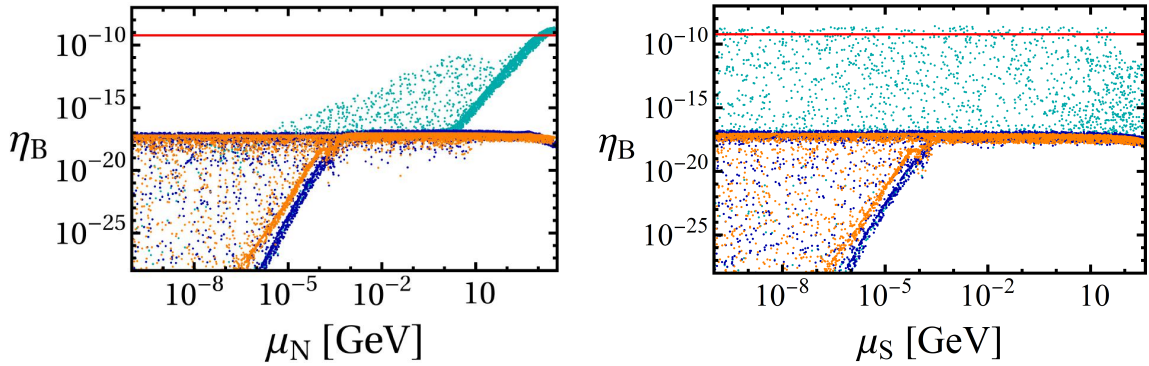


FIG. 1: Plot of the asymmetry generated in the ISS for the individual cases where no radiative corrections are considered (orange), where only \mathcal{N}_1 is considered (blue) and when both \mathcal{N}_1 and \mathcal{N}_2 are included (cyan). This was varied with μ_N (**left figure**) and μ_S (**right figure**). A resonant enhancement in the asymmetry occurs only if the next-to-leading order contributions are included. The orange horizontal line indicates the asymmetry required to fit observations.

Figure 2 plots the asymmetry when \mathcal{N}_2 is included and a clear resonant enhancement occurs for large values of μ_N . While the mass splitting is proportional to the decay width, it is also scaled by the Majorana mass μ_N . For small LNV the mass splitting will be much less than the decay width but for large values

$$\mu_N \left(\mathcal{Y}_D^\dagger \mathcal{Y}_D \right)_{ii} \rightarrow \frac{m_{N_i}}{8\pi} \left(\mathcal{Y}_D^\dagger \mathcal{Y}_D \right)_{ii} \simeq \Gamma_i \quad (80)$$

forcing a resonant enhancement to occur. In fig. 2 we distinguish between two different hierarchical cases for the Majorana masses: $\mu_N > \mu_S$ in purple and $\mu_S > \mu_N$ in green. The asymmetry in the resonant regime is independent of μ_S as in our setup this mass does not receive any radiative corrections. If a stricter setup was considered such that it did receive corrections (if, for example, we took an $SO(3)_{N_R} \times SO(3)_{S_L} \rightarrow SO(3)_{N_R+S_L}$ flavour symmetry) μ_S would require equivalently large masses in order to be placed in the required resonant regime. However, such large values of μ_S are outside the regime of validity required for the ISS and would spoil the guarantee of the parametrisation in eq. (56) to generate the required active neutrino masses. This follows as unlike μ_N , μ_S does not have a loop suppressed contribution to the active neutrino masses. Therefore we find that μ_S cannot contribute to the resonance required for MLFV-ISS.

Summarising, we find two criteria for successful MLFV-ISS resonant leptogenesis: (1)

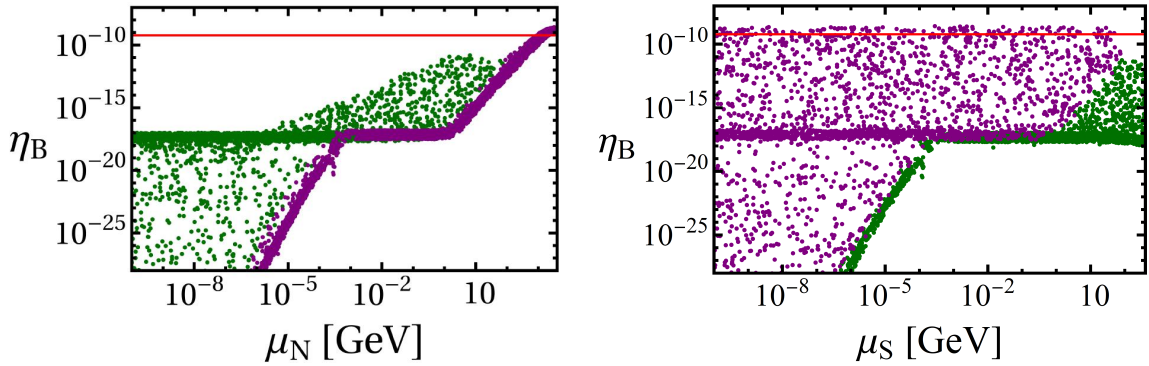


FIG. 2: Plot of the asymmetry generated in the ISS when both \mathcal{N}_1 and \mathcal{N}_2 are included, as a function of μ_N (**left figure**) and μ_S (**right figure**). Points in purple correspond to the regime where $\mu_N > \mu_S$, while points in green to $\mu_S < \mu_N$. A resonant enhancement of sufficient size is generated for *large* values of μ_N as long as the hierarchy $\mu_N > \mu_S$ is satisfied. In order to match active neutrino data, μ_S which generates a tree-level contribution must be less than ~ 100 GeV, whereas μ_N , which generates it at loop level, is allowed to be larger.

large values of the Majorana mass μ_N such that the mass splitting moves on resonance, and (2) the inclusion of spurion effects up to next-to-leading order in order to break flavour alignment and prevent only opposite mass splitting SNs from contributing to the asymmetry. This is illustrated in fig. 3 where the decay width and the mass splittings are plotted with the spurion corrections included. For large values of μ_N the opposite mass splitting SNs move further away from resonance whilst the same sign mass splitting SNs move onto resonance. This effect occurs both with \mathcal{N}_1 and \mathcal{N}_2 but, as discussed above, if only \mathcal{N}_1 is included then same sign mass splitting SNs combinations do not generate any flavoured asymmetry.

These conclusions were drawn for fixed values of certain parameters. Most importantly the Wilson coefficients were fixed such that $c_1 = 1/16\pi^2$, which we chose under the assumption that the high-scale dynamics arise from radiative effects. Increasing the size of the Wilson coefficients will increase the overall size of \mathcal{N}_2 from eq. (74), allowing for smaller values of μ_N by one or two orders of magnitude. Similarly, we fixed the lightest neutrino mass m_{ν_1} in our scans. Smaller values of the lightest neutrino mass will increase the hierarchy within $m_D^\dagger m_D$, which impacts the level of resonance through eq. (56). To illustrate this behaviour, in fig. 4 the asymmetry is plotted as a function of these two parameters where we

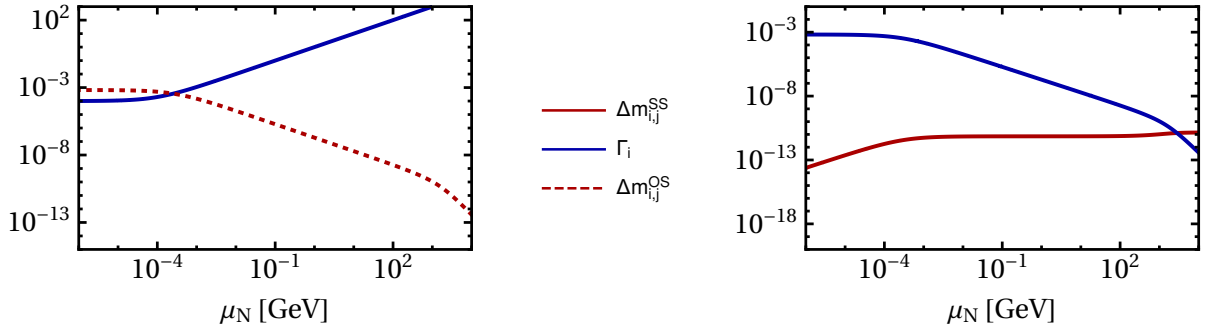


FIG. 3: Plot of the decay width $\Gamma_i \simeq \frac{m_i}{8\pi} \sum_l h_{li}^* h_{li}$ (blue) along with the mass splitting $\Delta m_{i,j}$ (red) as a function of μ_N for $\mu_S = 10^{-4}$ GeV and all radiative effects included. Here the mass splitting among opposite splitting SNs $\Delta m_{i,j}^{\text{OS}}$ (**left**) is compared to those with same sign splitting $\Delta m_{i,j}^{\text{SS}}$ (**right**) as defined in eqs. (40) and (41). While in both plots a region of resonance occurs, in the case on the left it occurs in a region of extremely strong washout c.f. fig. 5. The inclusion of radiative effects allows for a resonance to occur between SNs with same-sign mass splittings in a region of minimised washout such that asymmetry generation can occur. In this region heavy SNs of opposite sign mass splitting grow in mass difference and their contribution becomes irrelevant.

have fixed all other parameters to a benchmark point within the resonant region. From this figure we conclude that there is a preference for smaller values of neutrino mass $m_{\nu_1} \ll 0.1$ eV and if larger values of the Wilson coefficients were allowed, a larger region of parameter space would go on resonance.

Asymmetry generation is sufficient for large Majorana masses not simply because of the enhancement in the mass splitting. Due to the relationship between the Yukawa couplings required to satisfy active neutrino mixing data and the input parameters from eq. (56), larger values of the Majorana masses (for fixed Dirac mass m_R) results in a overall *decrease* in the couplings required to generate the same light neutrino masses which leads to less efficient washout of any generated asymmetry. Figure 5 plots the washout as a function of the two Majorana masses for the hierarchy $\mu_N > \mu_S$. Both the naïve washout $K_\alpha \propto \Gamma_i m_i / H(m_i)$ and the effective washout K_α^{eff} defined in eq. (68) (and relevant for scenarios with *small* LN violating parameters [82, 86, 87] due to the sensitivity to $2 \leftrightarrow 2$ scatterings) are plotted together.

While the naïve washout grossly overestimates the efficiency of washout, it is clear that for

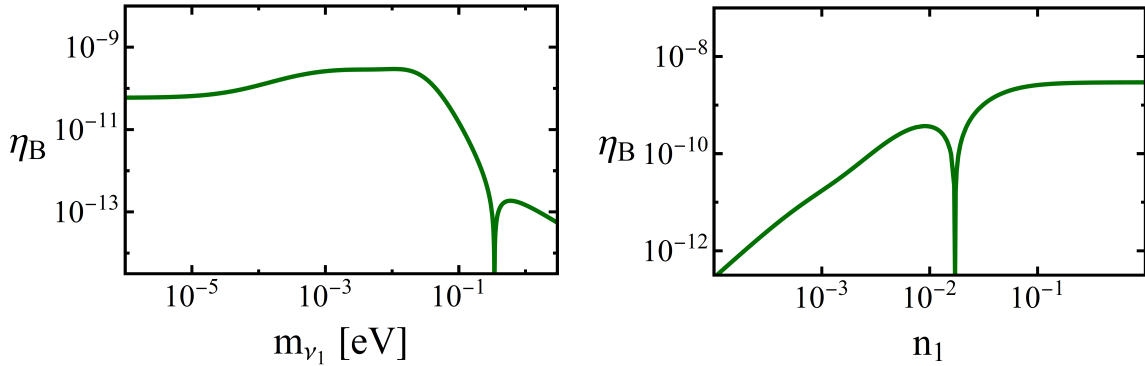


FIG. 4: Variation in the baryon asymmetry as a function of the lightest active neutrino mass m_{ν_1} (**left**) and varying the Wilson coefficient n_1 (**right**) for the case where all radiative spurion effects are included. In this scan we fixed $\theta_2^c = 0.7$, $\mu_S \simeq 10^{-1}$ GeV and $\mu_N \simeq 900$ GeV and in the left plot set $n_1 = 1/16\pi^2$ and $m_{\nu_1} = 0.01$ eV in the right plot. As the lightest neutrino mass is reduced (becomes hierarchical) the asymmetry freezes out. There is a slight preference for light neutrino masses of $\mathcal{O}(10^{-3} - 10^{-2})$ eV. Larger values for m_{ν_1} lead to a degeneracy amongst the light neutrino masses and decreases the mass splitting generated by the inclusion of \mathcal{N}_i decreasing the resonant enhancement. Increasing the size of the Wilson coefficient allows the mass splitting to be closer to resonance allowing for one or two orders of magnitude increased asymmetry.

large values of the LNV parameters palatable values of washout (albeit still very much in the strong washout regime) of $\mathcal{O}(10^3)$ or below are possible and therefore resonant leptogenesis is roughly feasible only in this specific region.

Figures. 6 and 7 plot the CP-asymmetry parameter to a specific lepton flavour¹³ α as a function of the Majorana masses. A ‘natural’ resonance occurs in the region of $\mu_i \simeq 10^{-4}$ GeV induced by $\Delta m_{i,j}^{\text{OS}}$ independent of the radiative spurion contributions, in agreement with [43]. However, this region is accompanied by a much larger effective washout and cannot accommodate sufficient asymmetry generation. In contrast only when both \mathcal{N}_1 and \mathcal{N}_2 are included does a clear second resonance peak form for large values of μ_N . Larger values of μ_N would cause $\mu_{\text{eff}} \gg M_R$ and the approximations involved in deriving eq. (50) and (56) would break down.

Finally in fig. 8 the asymmetry is varied against the complex angle θ_2^c for all three scenarios

¹³ Due to the anarchic nature of our scenario there is no preference for a specific lepton flavour.

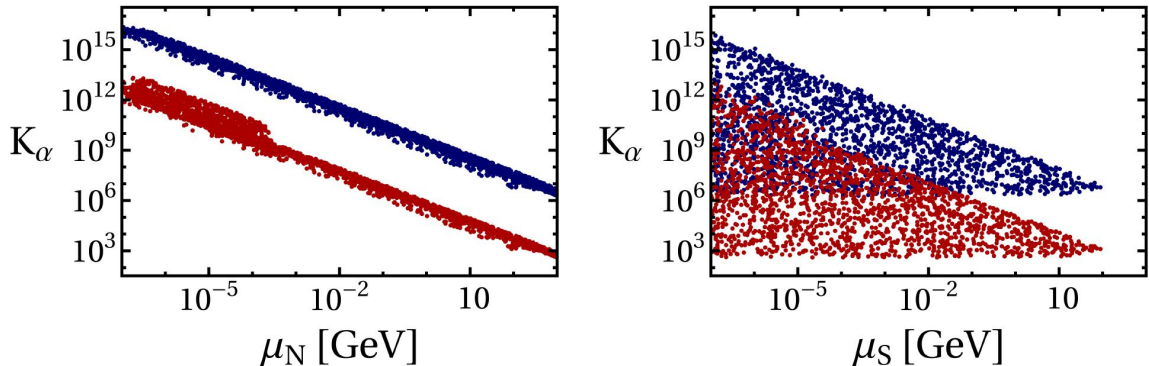


FIG. 5: Plot of the washout as a function of μ_N (**left**) and μ_S (**right**) in the scenario where $\mu_N > \mu_S$ relevant for resonant leptogenesis. In blue the naïve washout is plotted while in red the effective washout which is defined in eq. (68) relevant for situations with approximate lepton number conservation. As can be seen, naïvely the washout is overestimated by several orders of magnitude. In regions of large μ_N the effective washout is low enough (but still within the strong regime) for resonant leptogenesis to be feasible.

for a fixed benchmark point on resonance. In the case where no radiative effects are included, there is a slight dependence on the size of θ_2^c which can vary the asymmetry generated by one or two orders of magnitude. For small values of θ_2^c the asymmetry is generated by the CP-violating phase δ_{CP} within the low-energy mixing matrix. Similar behaviour occurs when \mathcal{N}_2 is included, with an overall preference for the range $0.1 < \theta_2^c < 1$. In the case where only \mathcal{N}_1 is included, we confirm its strong dependence on the angle θ_2^c similarly to the type-I scenario [52]. However, we note that in our case the asymmetry is not zero exactly unless $\theta_2^c = 0$. Asymmetry generation can only occur for non-zero values of θ_2^c independent of any low-energy CP violating phases as phases from U_{PMNS} cancel in the term $m_D^\dagger m_D$ in combination with the flavour alignment described above. Leptogenesis is viable both through the Dirac phase as well as high scale CPV but we note that within MLFV-ISS the region in which it is possible is very narrow.

B. $\ell_i \rightarrow \ell_j \gamma$ and MLFV-ISS

Here we briefly discuss the consequences of MLFV-ISS on low-energy cLFV processes, specifically the impact that the introduction of CPV has on predictions for $\ell_i \rightarrow \ell_j \gamma$. We also

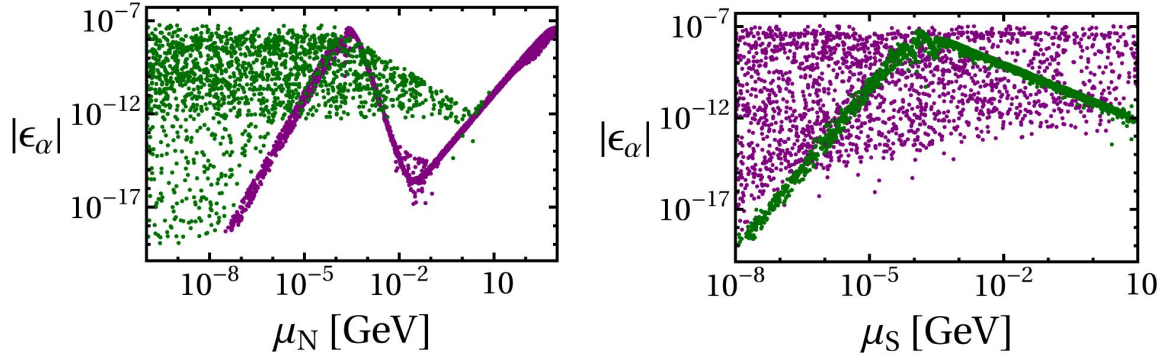


FIG. 6: Plot of the CP asymmetry into a specific flavour $\epsilon_\alpha = \sum_i \epsilon_\alpha^i$ generated in the ISS when both \mathcal{N}_1 and \mathcal{N}_2 are included, as a function of μ_N (**left figure**) and μ_S (**right figure**). Points in purple correspond to the regime where $\mu_N > \mu_S$, while points in green to $\mu_S < \mu_N$. At around 10^{-4} GeV a natural resonance occurs generated by $\Delta m_{i,j}^{\text{OS}}$ in agreement with [43]. Once radiative effects are included an additional resonance occurs for large values of μ_N and in the regime $\mu_N > \mu_S$.

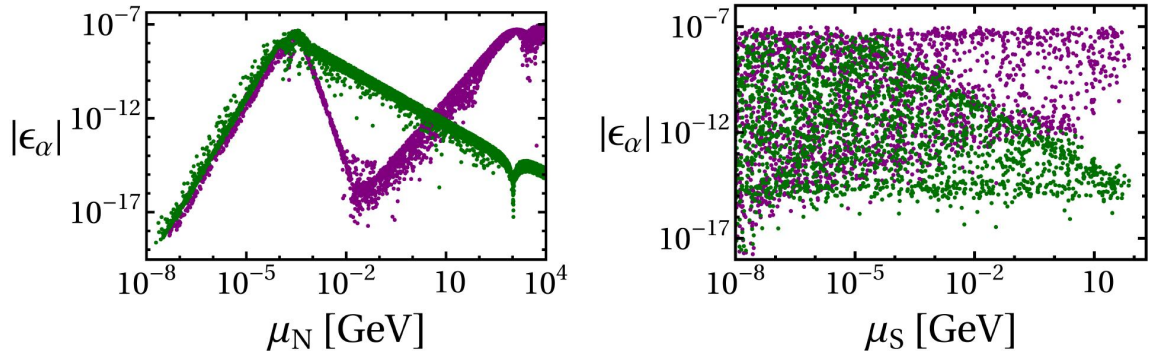


FIG. 7: Plot of the CP asymmetry into a specific flavour $\epsilon_\alpha = \sum_i \epsilon_\alpha^i$ generated in the ISS with no radiative effects included (green) and with \mathcal{N}_1 and \mathcal{N}_2 included (purple). This is varied with μ_N (**left figure**) and μ_S (**right figure**). A resonant enhancement in the asymmetry occurs only if the next-to-leading order contributions are included.

assess whether a future measurement of the region important for resonant leptogenesis will be possible. Similar to the MFV hypothesis of the quark sector, models of MLFV predict relationships between the rates for different charged lepton flavour decays.

In the SM effective field theory framework the process $\ell_i \rightarrow \ell_j \gamma$ arises from dimension six effective operators that contain $(\bar{\ell} \Gamma e_R)$ [46, 47, 83] where family indices have been

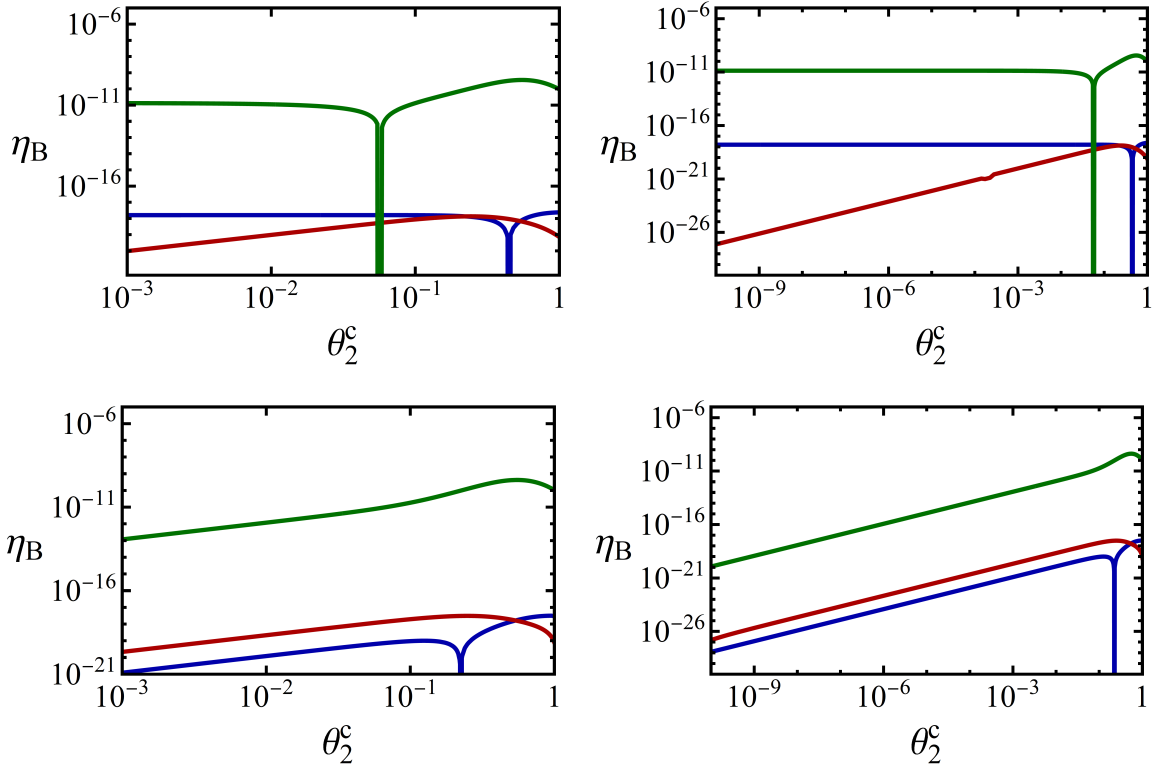


FIG. 8: Plot of the baryon asymmetry as a function of the complex angle θ_2^c for $\delta_{CP} = 3\pi/2$ (**top**) and $\delta_{CP} = 0$ (**bottom**). Here we have fixed $\mu_N \simeq 950$ GeV and $\mu_S \simeq 10$ GeV to be on resonance. In blue no radiative effects are included, in red only to leading order and in green next-to-leading order effects are included. The behaviour of the asymmetry as a function of the complex angle is clear. At small values it freezes out to that provided by the Dirac phase δ_{CP} however if only the leading radiative effects are included (red), the asymmetry tends to zero with decreasing θ_2^c even for non-zero δ_{CP} . This effect is similar to what occurs in the type-I MLFV scenario [52, 54, 88]. Asymmetry generation is possible both with low-energy phases as well as complex entries of the R matrix where we loosely find the criterion $0.1 \lesssim \theta_2^c \lesssim 1$ for sufficient asymmetry generation when $\delta_{CP} = 0$.

suppressed. These operators are not invariant under the flavour symmetry defined for MLFV in eq. (19). Insertion of spurion combinations transforming as $(\mathbf{3}, \bar{\mathbf{3}}, \mathbf{1}, \mathbf{1})$ make these terms formally invariant. At lowest order this is simply the spurion \mathcal{Y}_e . However, as we work in a basis where this matrix is diagonal, it does not contribute to flavour-violating processes. The lowest order spurion combination that makes the relevant operators flavour invariant

and contains non-diagonal entries is $\Delta\mathcal{Y}_e$, where

$$\Delta = \mathcal{Y}_D \mathcal{Y}_D^\dagger. \quad (81)$$

The combination transforms as $(\Delta\mathcal{Y}_e) \rightarrow \mathcal{U}_{\ell_L} (\Delta\mathcal{Y}_e) \mathcal{U}_{\ell_R}^\dagger$ as required.

A simple expression for the branching ratio is obtained [46] in the limit $m_{\ell_j} \ll m_{\ell_i}$,

$$B_{\ell_i \rightarrow \ell_j \gamma} = 384\pi^2 e^2 \frac{v^4}{4\Lambda_{\text{LFV}}^4} |\Delta_{ij}|^2 |C|^2 \quad (82)$$

where C accounts for a combination of Wilson coefficients of the relevant operators. As is conventional when considering cLFV in MLFV, we set $|C| = 1$. Note that in a specific UV-complete model based on MLFV these parameters will be fixed by the high-scale dynamics and may have a different magnitude.

In eq. (81) the only parameter which carries family indices is the spurion combination Δ_{ij} . Therefore useful predictive parameters for MLFV are ratios of branching ratios for different lepton flavour decays,

$$R_{(i,j)[k,l]} \equiv \frac{B_{\ell_i \rightarrow \ell_j \gamma}}{B_{\ell_k \rightarrow \ell_l \gamma}} = \frac{|\Delta_{ij}|^2}{|\Delta_{kl}|^2}. \quad (83)$$

In these ratios, the unknown scale of LFV (Λ_{LFV}) cancels out. While it can be identified with M_R in the ISS model, it is also possible that it could arise as the result of some unknown dynamics not directly related to the seesaw mechanism.

Many detailed explorations of cLFV in MLFV have been made for the minimal type-I seesaw scenario [46, 47, 53, 83], the results of which should also hold in the ISS. Here we briefly consider the impact of the complex angle θ_2^c and the Dirac phase δ_{CP} on the predictions for specific ratios of cLFV observables. In particular we compare the CP-conserving scenario (assumed in the simplest version of MLFV) with the CP-violating scenario and the size of deviation their inclusion introduces. As we have demonstrated that leptogenesis is viable with both the low-energy phase δ_{CP} and with the inclusion of the CP-violating angle θ_2^c , we analyse the two limiting cases where CPV arises solely from one of these angles.

Figure 9 plots three ratios of cLFV observables as a function of the lightest neutrino mass m_{ν_1} for $\theta_2^c = 0$ while varying δ_{CP} . The red and orange lines correspond to the CP-conserving scenarios $\delta_{CP} = 0$ or π , which allows for full reconstruction of \mathcal{Y}_D from low energy observables. The blue shaded region corresponds to all other values of δ_{CP} where the green line

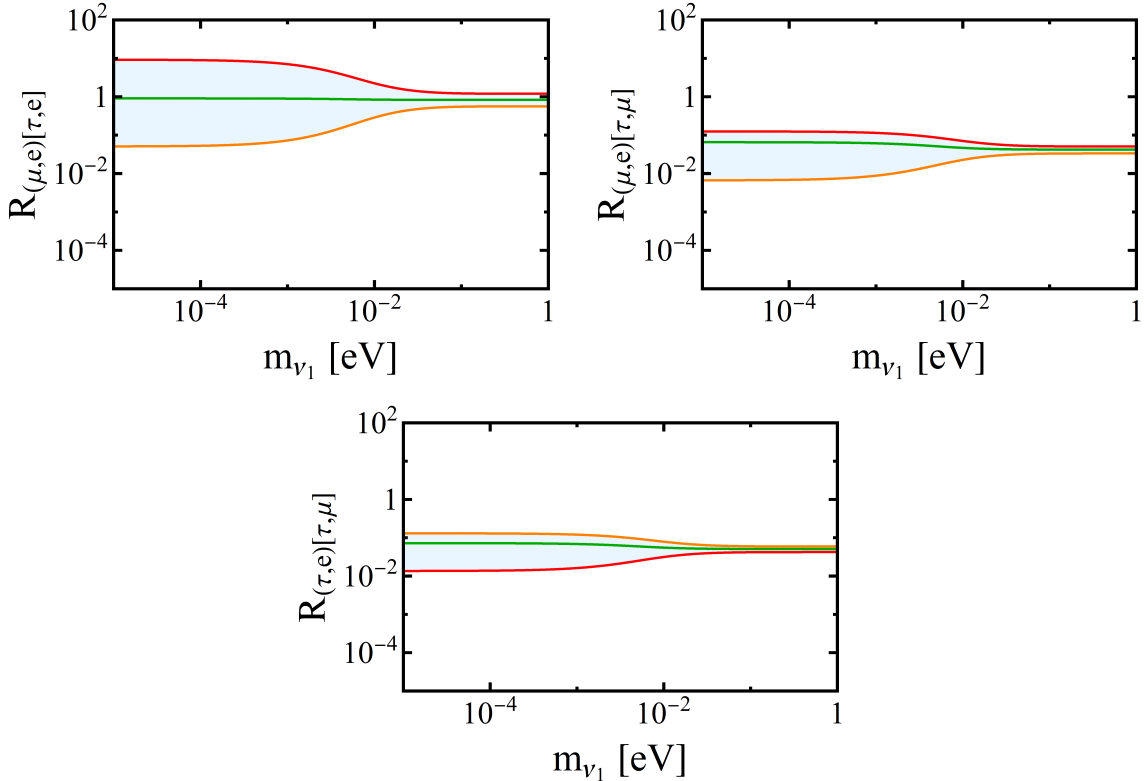


FIG. 9: Plot of the ratios $R_{(i,j)[k,l]}$ for various combinations of flavour initial and final states as a function of the lightest neutrino mass m_{ν_1} . Here the complex angle θ_2^c has been switched off but the low-energy phase δ_{CP} is varied. Lines in red and orange correspond to the CP-conserving cases $\delta_{CP} = 0$ and $\delta_{CP} = \pi$ respectively. In green is the maximally violating case of $\delta_{CP} = \pi/2$ or $\delta_{CP} = 3\pi/2$. The shaded blue region corresponds to $\delta_{CP} = (0, 2\pi) \setminus \{\pi/2, \pi, 3\pi/2\}$. All results are in full agreement with [47] for the CP-conserving cases.

specifically corresponds to the maximally CP-violating cases $\delta_{CP} = \pi/2$ or $3\pi/2$. The inclusion of CP-violating phases does not spoil the generic MLFV prediction that $R_{(\mu,e)[\tau,\mu]} \ll 1$ and $R_{(\tau,e)[\tau,\mu]} \ll 1$ in both the hierarchical and degenerate scenarios for the light neutrinos. A more potentially measurable effect occurs for the ratio $R_{(\mu,e)[\tau,e]}$, specifically for a hierarchical spectrum of light neutrinos. The CP-conserving case predicts either $R_{(\mu,e)[\tau,e]} > 1$ or $R_{(\mu,e)[\tau,e]} < 1$ depending on the choice of δ_{CP} , while the maximally CP-violating scenario predicts $R_{(\mu,e)[\tau,e]} \simeq 1$.

Similar plots are presented in fig. 10 where we plot the ratios as a function of the lightest neutrino mass m_{ν_1} for $\delta_{CP} = 0$ and varying θ_2^c . Once again a hierarchical spectrum of

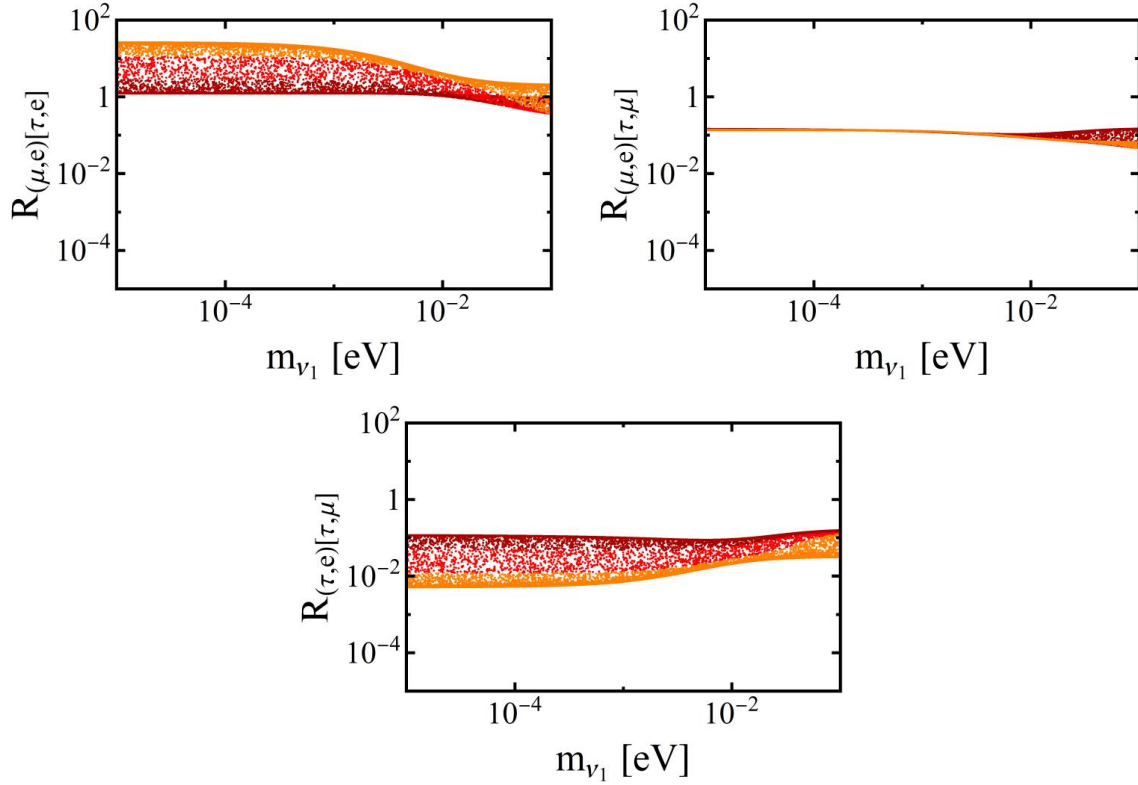


FIG. 10: Plot of the ratios $R_{(i,j)[k,l]}$ for various combinations of flavour initial and final states as a function of the lightest neutrino mass m_{ν_1} . Here the low-energy phase δ_{CP} has been switched off but the complex angle θ_2^c is varied. We find the same generic predictions as in the CP-conserving case of $R_{(\mu,e)[\tau,e]} > 1$ (**top-left**) $R_{(\mu,e)[\tau,\mu]} < 1$ (**top-right**) and $R_{(\tau,e)[\tau,\mu]} < 1$ (**bottom**). For the ratios $R_{(\mu,e)[\tau,e]}$ and $R_{(\tau,e)[\tau,\mu]}$ the introduction of CP-violation brings the ratios closer to one and this difference is most apparent with a hierarchical spectrum of light neutrinos. In orange $\theta_2^c < 0.1$, in red $0.1 < \theta_2^c < 0.3$ and in burgundy $\theta_2^c > 0.3$.

light neutrinos is required in order for CP-violating phases to have their most significant effect. The inclusion of θ_2^c does not spoil the generic predictions from the CP-conserving cases presented in fig. 9, however it is clear in the case of $R_{(\mu,e)[\tau,e]}$ and $R_{(\tau,e)[\tau,\mu]}$ that the inclusion of CP-violation (CP-conservation) moves the ratios closer (further) from one. Therefore future measurement of this ratio could constrain scenarios of MLFV that include CP violation.

Finally in fig. 11 the branching ratio $BR(\mu \rightarrow e\gamma)$ is plotted as a function of the LNV parameter μ_N . Here the cases where no CPV is present is distinguished from the cases where CPV arises from the low-energy observable δ_{CP} and from the complex angle θ_2^c . The LFV

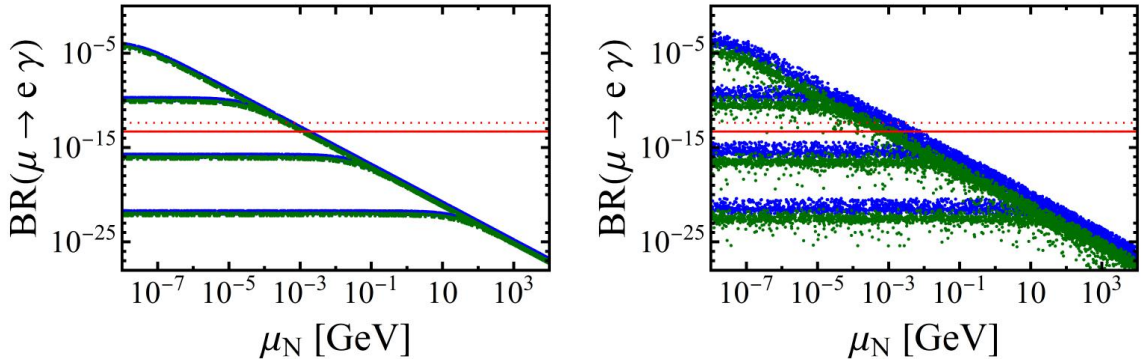


FIG. 11: Plot of the branching ratio $\text{BR}(\mu \rightarrow e\gamma)$ for $\theta_2^c = 0$ (left) and $0.1 < \theta_2^c < 1$ (right) as a function of μ_N . Points in blue correspond to the choice $\delta_{CP} = 0$ whereas points in green correspond to $\delta_{CP} = 3\pi/2$. In these plots the other LNV parameter μ_S has been fixed to the values 10^{-8} , 10^{-5} , 10^{-2} and 10 GeV. The ratio plateaus whenever $\mu_N < \mu_S$. The red dotted (solid) line corresponds to the current (future) sensitivity of MEG and MEG-II [89, 90], respectively, for this decay mode. Clearly, small values of the LNV parameters are experimentally accessible, while large values (necessary for MLFV-ISS resonant leptogenesis) correspond to a suppressed signal. The inclusion of low-scale CPV through the Dirac phase has no effect on the prediction, while CPV from θ_2^c can alter the prediction by approximately an order of magnitude.

scale has been fixed to $\Lambda_{\text{LFV}} = M_R = 1$ TeV and the LNV parameter μ_S has been fixed to the values described in the figure caption. The horizontal dotted (solid) red line corresponds to the current (future) sensitivity of MEG (MEG-II) [89, 90] for this decay process. Currently, MLFV-ISS has been excluded for very low values of μ_N and μ_S for which the scales of LNV $\Lambda_{\text{LNV}} = m_R^2/\mu_{\text{eff}}$ and LFV $\Lambda_{\text{LFV}} = m_R$ are most disparate.

Successful MLFV-ISS resonant leptogenesis, however, requires very large values of μ_N in order for sufficiently reduced washout to occur in combination with a resonant enhancement of the asymmetry. This corresponds to a reduction in the hierarchy between the LNV and LFV scale, suppressing the overall size of this cLFV decay. Therefore, while some overall predictions can be made within MLFV-ISS on the relative strength of various combinations of cLFV observables, a measurement of cLFV in near future experiments will be in conflict with the viable parameter space for MLFV-ISS leptogenesis in the absence of some additional mechanism to reduce the overall washout in this region.

C. Linear Seesaw (LSS)

For the LSS ($\mathcal{Y}_{\mu_S} = \mathcal{Y}_{\mu_N} = 0$) the LNV parameter arises from the (1, 3) and (3, 1) entry of the full neutrino mass matrix,

$$M_\nu = \begin{pmatrix} m_\nu^{\text{loop}} & m_D & m_L \\ m_D^T & 0 & M_R \\ m_L^T & M_R^T & 0 \end{pmatrix}. \quad (84)$$

From eq. (49) as long as $\mathcal{Y}_L \not\propto \mathbb{1}_3$ there is a radiative contribution to both the (2, 2) and (3, 3) entry which will break the $SO(3)^2$ invariance, leading to

$$\begin{aligned} \tilde{\mu}_N &= \mu_N (\mathcal{N}_1 + \mathcal{N}_2) \\ \tilde{\mu}_S &= \mu_S (\mathcal{S}_1 + \mathcal{S}_2), \end{aligned} \quad (85)$$

where

$$\begin{aligned} \mathcal{N}_1 &= n_1 \left(\mathcal{Y}_D^\dagger \mathcal{Y}_D + (\mathcal{Y}_D^\dagger \mathcal{Y}_D)^T \right), \\ \mathcal{N}_2 &= n_2^{(1)} \left(\mathcal{Y}_D^\dagger \mathcal{Y}_D \mathcal{Y}_D^\dagger \mathcal{Y}_D + (\mathcal{Y}_D^\dagger \mathcal{Y}_D \mathcal{Y}_D^\dagger \mathcal{Y}_D)^T \right) + n_2^{(2)} \left(\mathcal{Y}_D^\dagger \mathcal{Y}_D (\mathcal{Y}_D^\dagger \mathcal{Y}_D)^T \right) \\ &\quad + n_2^{(3)} \left((\mathcal{Y}_D^\dagger \mathcal{Y}_D)^T \mathcal{Y}_D^\dagger \mathcal{Y}_D \right) + n_2^{(4)} \left(\mathcal{Y}_D^\dagger \mathcal{Y}_e \mathcal{Y}_e^\dagger \mathcal{Y}_D + (\mathcal{Y}_D^\dagger \mathcal{Y}_e \mathcal{Y}_e^\dagger \mathcal{Y}_D)^T \right) \\ \mathcal{S}_1 &= s_1 \left(\mathcal{Y}_L^\dagger \mathcal{Y}_L + (\mathcal{Y}_L^\dagger \mathcal{Y}_L)^T \right), \\ \mathcal{S}_2 &= s_2^{(1)} \left(\mathcal{Y}_L^\dagger \mathcal{Y}_L \mathcal{Y}_L^\dagger \mathcal{Y}_L + (\mathcal{Y}_L^\dagger \mathcal{Y}_L \mathcal{Y}_L^\dagger \mathcal{Y}_L)^T \right) + s_2^{(2)} \left(\mathcal{Y}_L^\dagger \mathcal{Y}_L (\mathcal{Y}_L^\dagger \mathcal{Y}_L)^T \right) \\ &\quad + s_2^{(3)} \left((\mathcal{Y}_L^\dagger \mathcal{Y}_L)^T \mathcal{Y}_L^\dagger \mathcal{Y}_L \right) + s_2^{(4)} \left(\mathcal{Y}_L^\dagger \mathcal{Y}_e \mathcal{Y}_e^\dagger \mathcal{Y}_L + (\mathcal{Y}_L^\dagger \mathcal{Y}_e \mathcal{Y}_e^\dagger \mathcal{Y}_L)^T \right). \end{aligned} \quad (86)$$

As before, we consider separately the cases where no corrections are included, corrections are included at leading order and corrections are included at next-to-leading order.

For the ISS scenario the corrections to the Majorana mass $\tilde{\mu}_N$ were proportional to the non-zero bare mass μ_N itself and scaled as μ_N . For the LSS, by contrast, we operate in a regime where an explicit Majorana mass term in the Lagrangian is forbidden. However, flavour-invariant combinations such as $\mathcal{Y}_D^\dagger \mathcal{Y}_D$ and $\mathcal{Y}_L^\dagger \mathcal{Y}_L$ transform in the necessary way to induce mass terms for each SN.

Here the dimensionful parameters μ_N and μ_S cannot be identified with bare Majorana mass terms. Rather, they arise from the unknown UV complete dynamics. As we remain agnostic about these dynamics, yet under the MLFV Ansatz we must include such terms,

we choose to fix the values of μ_N and μ_S in some plausible way. For example, it seems reasonable to take $\mu_i \simeq v^2/M_X$, which would be true if μ_i arose from some effective coupling with the SM Higgs doublet mediated by a heavy new particle X , generating an operator similar to the Weinberg operator.

We fix these parameters to $\mu_N = \mu_S = 1$ GeV which, in the example given above, would arise if $m_X \simeq \mathcal{O}(10 - 1000)$ TeV depending on the strength of the relevant couplings. We also make the reasonable assumption that this mass scale is independent from m_L .

Figure 12 plots the asymmetry generated as a function of m_L in the three scenarios considered. Points in blue correspond to the asymmetry without including \mathcal{N}_i and \mathcal{S}_i . As discussed previously near eq. (47), in this regime (where all the SNs have identical masses) the self-energy contribution to the CP-asymmetry is switched off but a non-zero asymmetry is generated from the vertex contribution and differences in the decay widths of each SN. The most asymmetry (albeit much too small) is generated in the region where the washout is minimised, as shown fig. 13, in agreement with [43].

Points in orange correspond to spurion insertions at lowest order and points in cyan include all relevant terms. Now, due to the inclusion of the radiative Majorana masses, mass splittings occur between the six heavy SNs. The self-energy component of eq. (43) turns on and increases the overall CP-asymmetry (due to a resonance between the SN masses) by several orders of magnitude. Here, including the next-to-leading order contributions does not change the size of the asymmetry generated. By contrast with with MLFV-ISS, the flavour mis-alignment between m_D and m_L generates non-diagonal real entries in eq. (39) at lowest order which also allows for larger values of ε_i^α .

Figure 14 plots the CP-asymmetry into a specific lepton flavour α in the three scenarios, where once again due to the anarchic nature each flavour has the same behaviour and overall size. It is clear that, for all values of m_L , the CP-asymmetry is orders of magnitude larger when the radiative Majorana masses are included. In other words, for the entire region of the parameter space, roughly the same resonant enhancement is occurring. This forced-resonance is occurring as the mass splitting between the heavy SNs is related to the small Majorana parameters,

$$\begin{aligned} m_{N_j} &\simeq m_R + \frac{\tilde{\mu}_N}{2} + \frac{\tilde{\mu}_S}{2} \\ m_{N_i} &\simeq m_R - \frac{\tilde{\mu}_N}{2} - \frac{\tilde{\mu}_S}{2} \end{aligned} \tag{87}$$

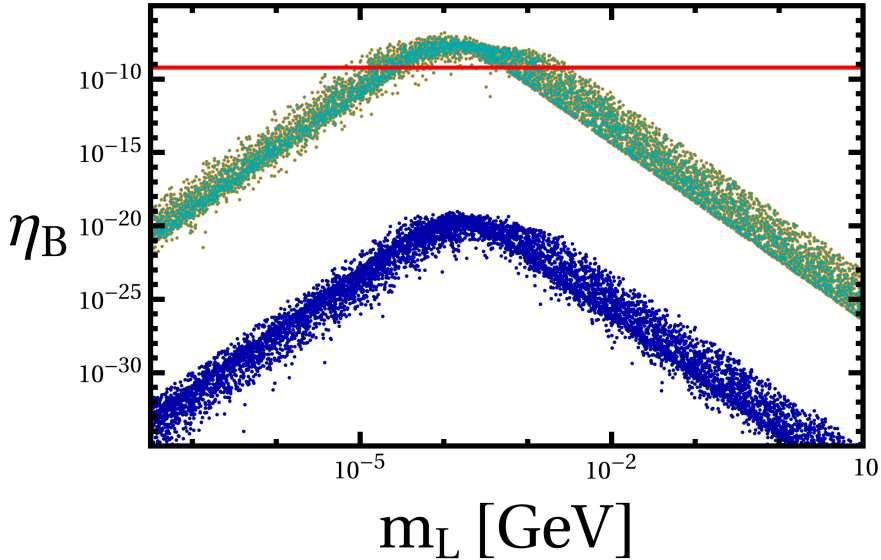


FIG. 12: Plot of the asymmetry generated in the LSS for the three scenarios as a function of the LNV parameter m_L in GeV. Points in blue correspond to no radiative corrections, points in orange are when \mathcal{N}_1 and \mathcal{S}_1 are included and points in cyan include all terms. Contrary to the case of MLFV-ISS, corrections at leading order are sufficient to generate the necessary asymmetry. The case without any radiative corrections is highly suppressed as the self-energy contributions to ε_i^α are identically zero. However a non-zero asymmetry is generated due to the differences in the decay widths generating slight deviations in the vertex contribution for each SN, c.f. eq. (47).

leading to

$$\Delta m_{ij} = m_{N_i} - m_{N_j} = \tilde{\mu}_N + \tilde{\mu}_S = \mu_N n_1 \left(\mathcal{Y}_D^\dagger \mathcal{Y}_D \right) + \mu_S s_1 \left(\mathcal{Y}_L^\dagger \mathcal{Y}_L \right) \propto \Gamma_{i,j}, \quad (88)$$

where we take the parameters $\tilde{\mu}_N$ and $\tilde{\mu}_S$ to be independent of m_L . Therefore the same level of resonant enhancement occurs for the entire parameter space. Unlike with MLFV-ISS, both $\Delta m_{i,j}^{\text{OS}} \neq 0$ and $\Delta m_{i,j}^{\text{SS}} \neq 0$ occurs at lowest order in the corrections and they both contribute to the asymmetry generated.

To illustrate this, fig. 15 plots the mass splitting Δm_{ij} and the decay width Γ_i as a function of m_L . The parameter which most significantly impacts the level of resonance (where the mass splitting overlaps with the decay width) is the combination of $\mu_N n_i$ and $\mu_S s_i$. The resonant enhancement is maximised when

$$\Delta m_{i,j} \simeq \Gamma_{i,j} = \frac{(h^\dagger h)}{8\pi} m_{N_i} \simeq 40 (h^\dagger h) \text{ GeV.} \quad (89)$$

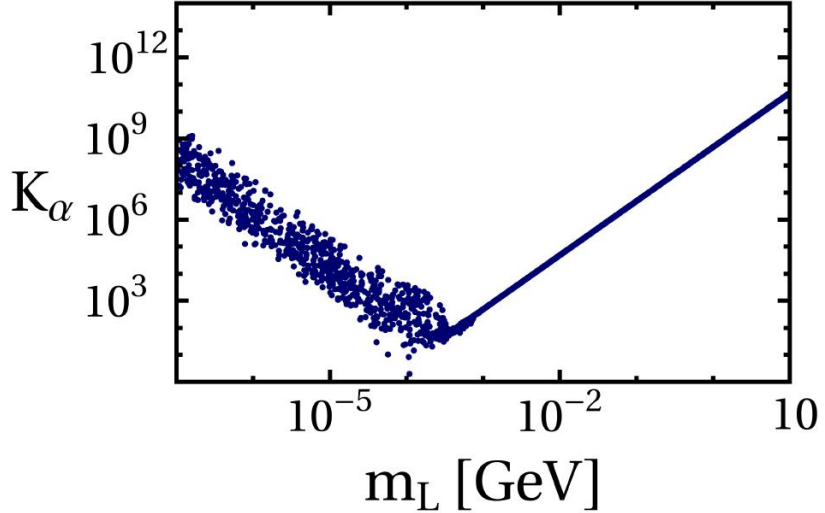


FIG. 13: Plot of the effective washout to a specific lepton flavour K_α generated in the LSS as defined in eq. (68). We find the washout is minimised for $m_L \simeq \mathcal{O}(10^{-5} - 10^{-3})$ GeV in agreement with [43]. The washout which is related to the Yukawa couplings in the mass basis of the heavy SNs from eq. (39), is dominantly controlled by m_L (m_D) when $m_L > m_D$ ($m_D > m_L$). For large values of m_L the washout is not dependent on the size of the complex parameter a_2^c whereas for small values where m_D dominates, different values of a_2^c can produce different values of washout for the same choice of m_L .

This places constraints on the overall size of the combination $\mu_N n_i$ and $\mu_S s_i$ required in order for enough asymmetry to be generated. While this forced resonance occurs, in order for it to significantly impact the asymmetry, it relies on the radiative Majorana masses generated arising from a scale around $\mathcal{O}(1 - 1000)$ GeV.

In fig. 16 we vary the lightest neutrino mass m_{ν_1} and the Wilson coefficients for fixed choices of the other parameters as described in the figure caption. We find similar conclusions to MLFV-ISS where large values of the light neutrino mass m_{ν_1} correspond to smaller asymmetry generation. Masses less than $\mathcal{O}(10^{-3})$ eV maximise the asymmetry generated. Larger values for the Wilson coefficient leads to a larger asymmetry and allows for a wider range of values of m_L to produce the necessary asymmetry along with smaller values for the CPV parameters.

Based on these two scenarios, we conclude that successful MLFV resonant leptogenesis will also occur if the ISS and LSS were operative together. Appropriate choices for the now

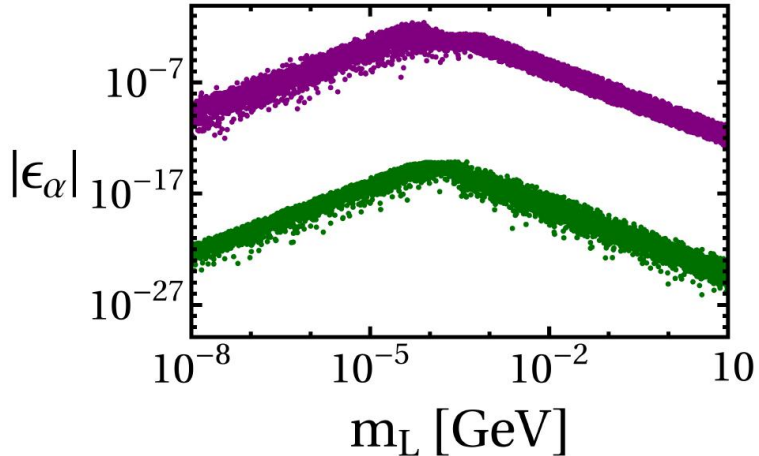


FIG. 14: Plot of the CP-asymmetry to a specific lepton flavour α as a function of m_L .

Points in green correspond to when \mathcal{N}_i and \mathcal{S}_i are not included and points in purple correspond to when they are included (at lowest order and next-to-leading order the points are identical). Clearly a resonance due to their inclusion increases the overall CP-asymmetry by many orders of magnitude. The mass splittings induced in this scenario are directly proportional to the decay widths and therefore for any choice of m_L the mass splittings will always be in a resonant regime.

three LNV parameters based on the two scenarios here will allow for minimised washout with mass splittings related to the heavy SN decay widths for the necessary resonance to occur. However, as resonant leptogenesis is already feasible [43] in this scenario without the need for radiative resonant leptogenesis, we do not consider this scenario further.

Finally, in fig. 17 we plot the behaviour of the asymmetry as a function of the complex component of the C matrix when low-energy CPV is included and when it is not. Similarly to the ISS case, asymmetry generation can be predominately due to either the Dirac phase δ_{CP} or the complex component a_2^c of the C matrix. We find consistent behaviour for the baryon asymmetry as these CPV parameters are taken to zero. It is clear from both figs. 12 and 17 that a larger portion of the parameter space provides the necessary asymmetry generation allowing for smaller sizes of the CPV parameters, decreasing their contribution to flavour-violating processes.

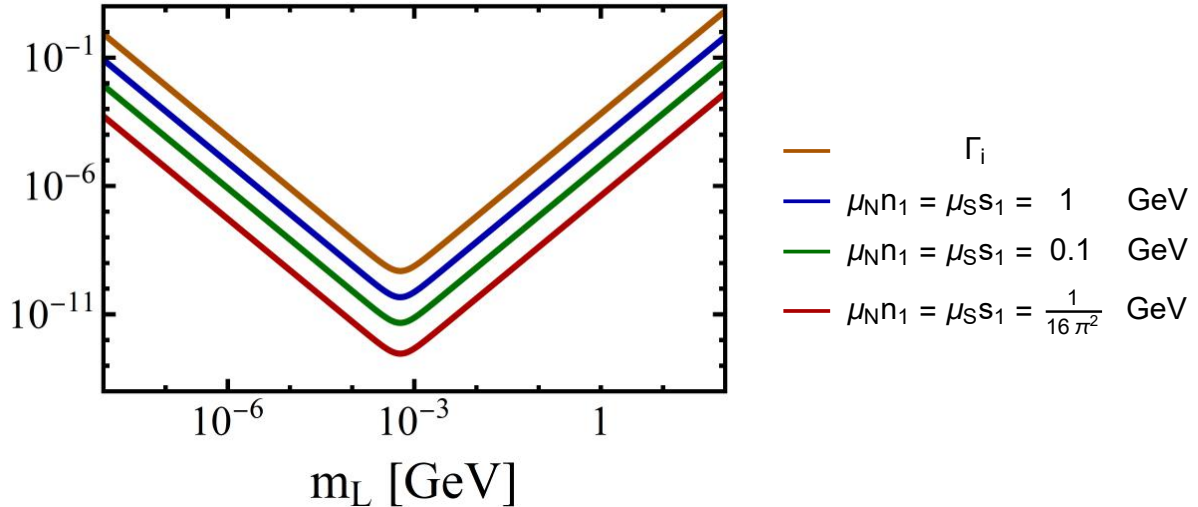


FIG. 15: Plot of the mass splitting Δm_{ij} as a function of m_L in GeV when \mathcal{N}_1 and \mathcal{S}_1 are included. In red $\mu_N n_i = \mu_S s_i = 1/(4\pi)^2$ GeV, in green $\mu_N n_i = \mu_S s_i = 0.1$ GeV and in blue $\mu_N n_i = \mu_S s_i = 1$ GeV. This is plotted against the decay width $\Gamma_{i,j}$ in brown. As the combination $\mathcal{N}_1 + \mathcal{S}_1 \propto \Gamma_{i,j}$ the mass splitting induced will always be on resonance independent of the value of m_L . Here there is no distinction between $\Delta m_{i,j}^{\text{SS}}$ and $\Delta m_{i,j}^{\text{OS}}$ and they both behave in a similar way.

D. $\ell_i \rightarrow \ell_j \gamma$ and MLFV-LSS

Once again we briefly consider the prospects of detection of MLFV-LSS through cLFV processes. Unlike in the MLFV-ISS scenario a much less tuned region of parameter space is required in order to generate the necessary baryon asymmetry which may lead to improved detection prospects.

As before we require insertions of spurions transforming as a $(\mathbf{3}, \bar{\mathbf{3}}, \mathbf{1}, \mathbf{1})$ in order to make the necessary dimension six effective operators invariant. Off-diagonal terms are required in order for LFV processes to occur. The lowest order combination which satisfies this is once again

$$\Delta \mathcal{Y}_e = \mathcal{Y}_D \mathcal{Y}_D^\dagger \mathcal{Y}_e + \mathcal{Y}_L \mathcal{Y}_L^\dagger \mathcal{Y}_e. \quad (90)$$

While the combination $\mathcal{Y}_L \mathcal{Y}_L^\dagger$ may transform in the correct way, it does not contain the necessary off-diagonal terms in our scan and therefore cLFV will once again be controlled by $\mathcal{Y}_D \mathcal{Y}_D^\dagger$.

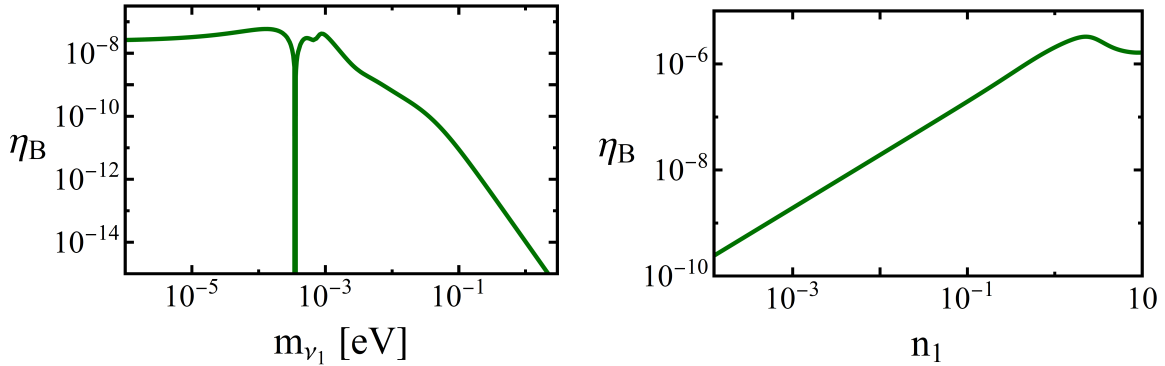


FIG. 16: Variation in the baryon asymmetry as a function of the lightest active neutrino mass m_{ν_1} (**left**) and varying the Wilson coefficients n_i and s_i (**right**) for the case where all radiative spurion effects are included. In this scan we fixed $a_2^c = 0.7$ and in the left plot set $n_i, s_i = 1/16\pi^2$ whereas we fixed $m_{\nu_1} = 0.01$ eV in the right plot. In both plots similar behaviour compared to MLFV-ISS is found.

Figure 18 plots the three ratios of cLFV observables as in the ISS case for the scenario where $a_2^c = 0$ while δ_{CP} is varying. Similar predictions on the ratio $R_{(\mu,e)[\tau,\mu]}$ are made compared to the ISS scenario and therefore the branching ratio $\text{BR}(\tau \rightarrow \mu\gamma)$ should be larger by one or two orders of magnitude compared to $\text{BR}(\mu \rightarrow e\gamma)$. Here there is a cancellation in $\tau \rightarrow e\gamma$ for specific values of the lightest neutrino m_{ν_1} and the phase δ_{CP} . In these regions a strong suppression of this channel is predicted. Outside the regions of strong cancellation the LSS similarly predicts $R_{(\tau,e)[\tau,\mu]} < 1$ but always predicts $R_{(\mu,e)[\tau,e]} > 1$ unlike the type-I and ISS case where this varied depending on the value of δ_{CP} . As before the introduction of CPV appears to bring the ratios closer together.

Figure 19 plots the ratios of cLFV observables in the scenario where $\delta_{CP} = 0$ and a_2^c is varied. We find that overall the presence of the CPV parameter becomes more impactful for larger values of the lightest neutrino mass, while for a hierarchical spectrum its impact is less significant. Overall similar predictions to the case where δ_{CP} was varied are obtained and a significant portion of the parameter space is not strongly sensitive to the presence of CPV. This implies the inclusion of CPV necessary for leptogenesis does not significantly modify the predictions given by the CP-conserving case.

Finally, fig. 20 plots the predictions for the branching ratio $\text{BR}(\mu \rightarrow e\gamma)$ as a function of the LNV parameter m_L for $\Lambda_{\text{LFV}} = 1$ TeV. As before, we plot cases with no CPV violation

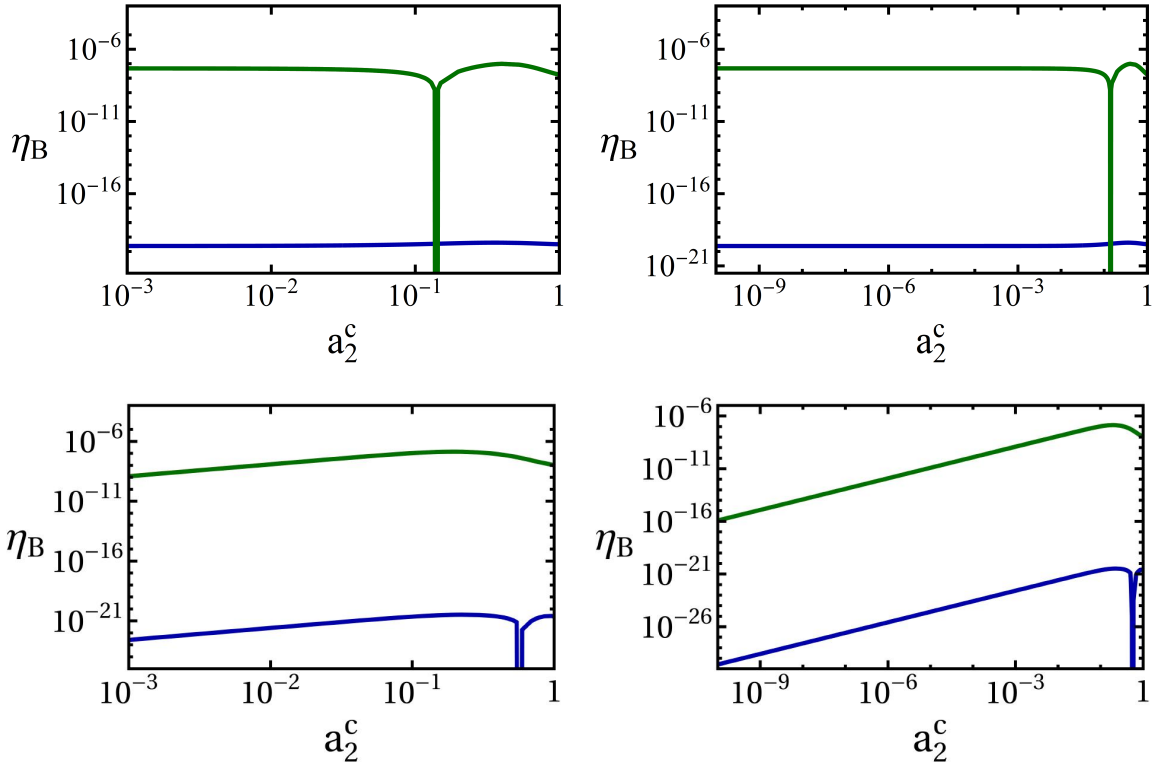


FIG. 17: Plot of the baryon asymmetry as a function of the complex parameter a_2^c for $\delta_{CP} = 3\pi/2$ (**top**) and $\delta_{CP} = 0$ (**bottom**). Here we have fixed $m_L \simeq 10^{-4}$ GeV to be in a region with sufficient washout suppression for necessary asymmetry generation. In blue no radiative effects are included and in green is the scenario where spurion effects are included. The behaviour of the asymmetry as a function of the complex angle has consistent behaviour as it is taken to zero. As before asymmetry generation is possible both with low-energy phases as well as complex entries of the C matrix where smaller values of a_2^c are allowed compared to the ISS scenario.

and cases in which CPV is present. The dotted (solid) red line corresponds to the current (future) limit placed by MEG(MEG-II). Due to the LSS parameterisation in eq. (58), the Dirac-mass matrix m_D is now inversely related to m_L and has a larger suppression as m_L is increased compared to increasing the Majorana masses in the ISS scenario. While small values of m_L are currently constrained, the region $10^{-5} \lesssim m_L/\text{GeV} \lesssim 10^{-3}$ required in order to account for baryogenesis will not be probed in near-future experiments. This roughly corresponds with the LNV scale $\Lambda_{\text{LNV}} \simeq (10^6 - 10^4)$ GeV which will not be probed in the near future. This is in agreement with the estimates found in [47] for the necessary LNV

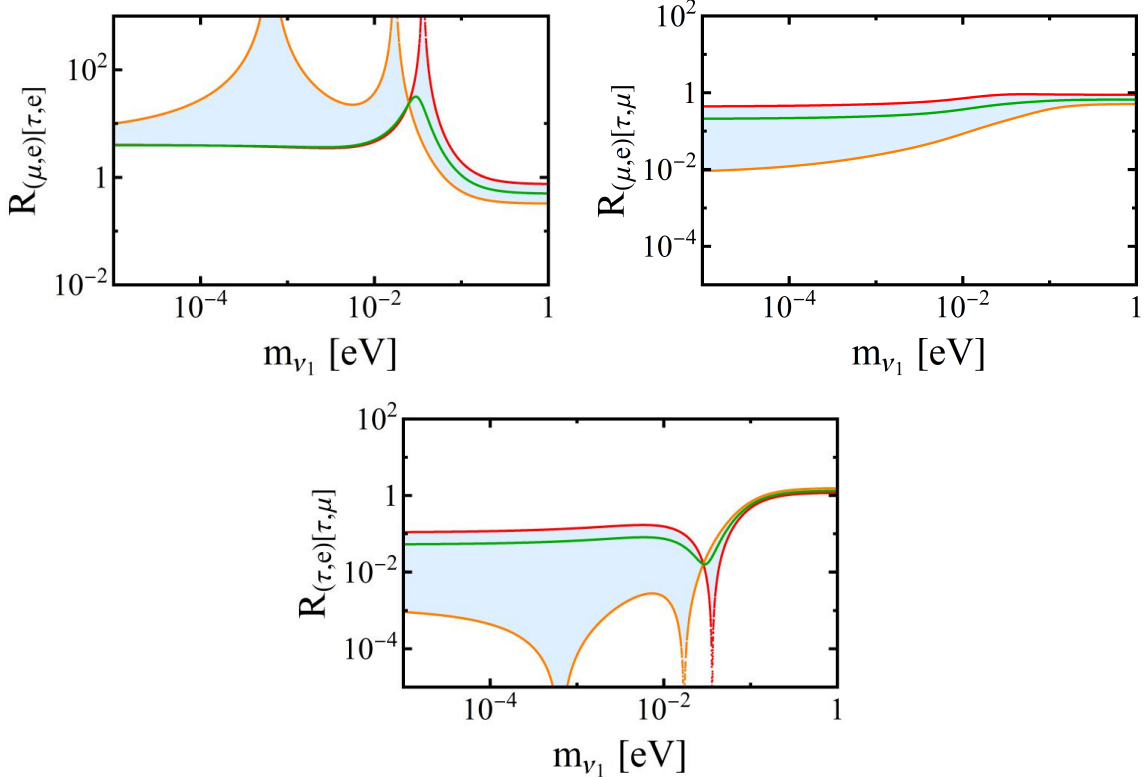


FIG. 18: Plot of the ratios $R_{(i,j)[k,l]}$ for various combinations of flavour initial and final states as a function of the lightest neutrino mass m_{ν_1} . Here the complex parameter a_2^c has been switched off but the low-energy phase δ_{CP} is varied. Lines in red and orange correspond to the CP-conserving cases $\delta_{CP} = 0$ and $\delta_{CP} = \pi$ respectively. In green is the maximally violating case of $\delta_{CP} = \pi/2$ or $\delta_{CP} = 3\pi/2$. The shaded blue region corresponds to $\delta_{CP} = (0, 2\pi) \setminus \{\pi/2, \pi, 3\pi/2\}$.

scale for a given LFV scale to be probed. A future measurement of the process $\mu \rightarrow e\gamma$ may rule out LSS as a leptogenesis candidate in the absence of additional physics introduced to lower the overall strength of the washout present for smaller values of m_L .

V. CONCLUSION

We have studied a well-motivated way in which small mass splittings between heavy SNs from different families may arise, within both the ISS and LSS frameworks, such that leptogenesis is possible despite the strong washout present in the theory. Previously it was found that while a mass splitting naturally exists for the ISS it is not sufficient in order

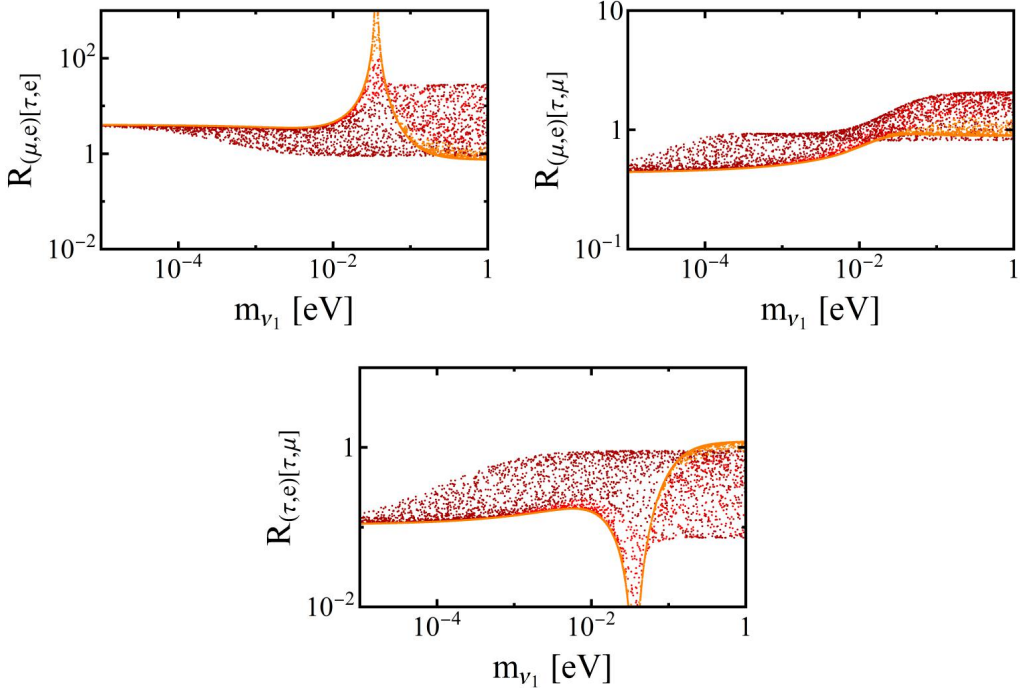


FIG. 19: Plot of the ratios $R_{(i,j)[k,l]}$ for various combinations of flavour initial and final states as a function of the lightest neutrino mass m_{ν_1} . Here the low-energy phase δ_{CP} has been switched off but the complex parameter a_2^c is varied. We find the same generic predictions as in the CP-conserving case of $R_{(\mu,e)[\tau,e]} > 1$ (**top-left**) $R_{(\mu,e)[\tau,\mu]} \lesssim 1$ (**top-right**) and $R_{(\tau,e)[\tau,\mu]} \lesssim 1$ (**bottom**). Similar to the scenario above a cancellation occurs for the process $\tau \rightarrow e\gamma$ for specific values of the lightest neutrino mass m_{ν_1} . In orange $a_2^c < 0.1$, in red $0.1 < a_2^c < 0.3$ and in burgundy $a_2^c > 0.3$.

for resonant leptogenesis to occur. For the LSS the degeneracy amongst the SNs at the high scale prevents significant asymmetry generation. While leptogenesis is feasible when all LNV terms are switched on (the ISS+LSS case) we explore the potential for ISS or LSS leptogenesis to occur independently, where additional symmetries may prevent both terms from existing.

In the context of broken flavour symmetries and the MLFV hypothesis, a degeneracy amongst the heavy SNs is naturally produced, for the purposes of having a predictive theory. The degeneracy is then broken by higher-order spurion VEV contributions, leading to a parameter region consistent with resonant asymmetry generation. In order for the desired splitting to occur in the intended way during cosmological evolution, the critical tempera-

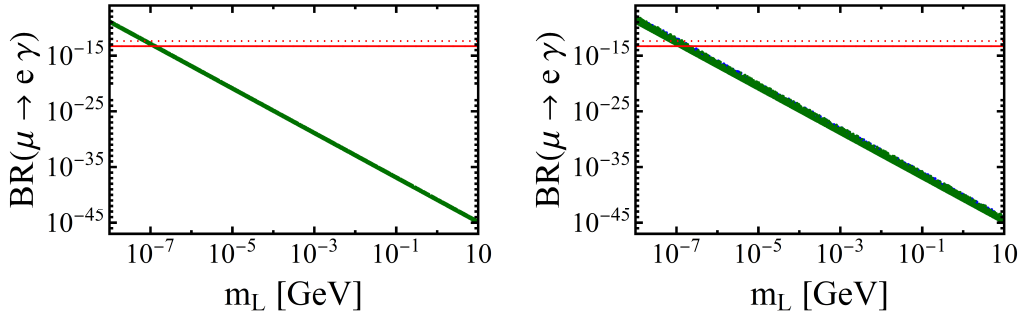


FIG. 20: Plot of the branching ratio of $\mu \rightarrow e\gamma$ for $\theta_2^c = 0$ (**left**) and $0.1 < a_2^c < 1$ (**right**) as a function of m_L . Points in blue correspond to the choice $\delta_{CP} = 0$ whereas points in green correspond to $\delta_{CP} = 3\pi/2$. The red dotted(solid) line corresponds to the current(future) sensitivity of MEG and MEG-II [89, 90] respectively for this decay mode.

Currently very small values of the LNV parameter are probed for MLFV-LSS which correspond to a very large separation of the LNV and LFV scales. In order to allow for necessary asymmetry generation we require approximately $10^{-5} \lesssim m_L/\text{GeV} \lesssim 10^{-3}$ which will not be probed by MEG-II in the near future. The inclusion of CPV of any type does not significantly impact the predictions.

ture at which the spurions acquire their non-zero VEVs must be assumed to be above the scale of thermal leptogenesis.

We found that for MLFV-ISS only a small region of very large Majorana masses is able to generate the required asymmetry. Here asymmetry generation requires next-to-leading order corrections to be included, therefore suppressing the overall size of the CP-asymmetry generated per decay of SN. We briefly discussed the impact of CPV on potential low-energy observables, in particular how various ratios of cLFV decays are impacted compared to the CP conserving MLFV scenario. The region compatible with leptogenesis will not, however, be probed by current and near future cLFV experiments.

For MLFV-LSS a large region of parameter space is capable of satisfying the resonance condition simultaneously with the minimised washout required for successful asymmetry generation. Here corrections at lowest order are not flavour aligned and therefore much larger values of the CP-asymmetry are possible compared to the ISS. Similarly, we studied the impact of CPV on cLFV observables and find that small deviations occur due to their inclusion. In this case, relatively small values of the CPV parameters allow for sufficient

asymmetry generation allowing for even smaller deviations as compared to the ISS case.

In both cases we estimated the impact of the lightest neutrino mass m_{ν_1} on the asymmetry generated. We find a clear preference for small values where the light neutrinos are hierarchical and estimate that $m_{\nu_1} \lesssim 10^{-2}$ eV is required. Unsurprisingly we find that MLFV leptogenesis favours larger values for the Wilson coefficients related to the Majorana mass corrections in both scenarios.

ACKNOWLEDGMENTS

This work was supported in part by the Australian Research Council. TPD thanks Vincenzo Cirigliano and Luca Merlo for clarifications related to MLFV. TPD is grateful to Uli Felzmann for access to computing hardware on which our scans were conducted.

[1] P. Minkowski, $\mu \rightarrow e\gamma$ at a Rate of One Out of 10^9 Muon Decays?, *Phys. Lett.* **67B**, 421 (1977).

[2] T. Yanagida, Horizontal Symmetry and Masses of Neutrinos, *Proceedings: Workshop on the Unified Theories and the Baryon Number in the Universe: Tsukuba, Japan, February 13-14, 1979*, Conf. Proc. **C7902131**, 95 (1979).

[3] M. Gell-Mann, P. Ramond, and R. Slansky, Complex Spinors and Unified Theories, *Supergravity Workshop Stony Brook, New York, September 27-28, 1979*, Conf. Proc. **C790927**, 315 (1979), arXiv:1306.4669 [hep-th].

[4] R. N. Mohapatra and G. Senjanovic, Neutrino Mass and Spontaneous Parity Violation, *Phys. Rev. Lett.* **44**, 912 (1980).

[5] S. L. Glashow, The Future of Elementary Particle Physics, *Cargese Summer Institute: Quarks and Leptons Cargese, France, July 9-29, 1979*, NATO Sci. Ser. B **61**, 687 (1980).

[6] M. Fukugita and T. Yanagida, Baryogenesis Without Grand Unification, *Phys. Lett.* **B174**, 45 (1986).

[7] W. Buchmuller, P. Di Bari, and M. Plumacher, Leptogenesis for pedestrians, *Annals Phys.* **315**, 305 (2005), arXiv:hep-ph/0401240 [hep-ph].

[8] W. Buchmuller, R. D. Peccei, and T. Yanagida, Leptogenesis as the origin of matter, *Ann.*

Rev. Nucl. Part. Sci. **55**, 311 (2005), arXiv:hep-ph/0502169 [hep-ph].

[9] P. Di Bari, An introduction to leptogenesis and neutrino properties, Contemp. Phys. **53**, 315 (2012), arXiv:1206.3168 [hep-ph].

[10] S. Davidson and A. Ibarra, A Lower bound on the right-handed neutrino mass from leptogenesis, Phys. Lett. **B535**, 25 (2002), arXiv:hep-ph/0202239 [hep-ph].

[11] G. F. Giudice, A. Notari, M. Raidal, A. Riotto, and A. Strumia, Towards a complete theory of thermal leptogenesis in the SM and MSSM, Nucl. Phys. **B685**, 89 (2004), arXiv:hep-ph/0310123 [hep-ph].

[12] F. Vissani, Do experiments suggest a hierarchy problem?, Phys. Rev. **D57**, 7027 (1998), arXiv:hep-ph/9709409 [hep-ph].

[13] J. D. Clarke, R. Foot, and R. R. Volkas, Electroweak naturalness in the three-flavor type I seesaw model and implications for leptogenesis, Phys. Rev. **D91**, 073009 (2015), arXiv:1502.01352 [hep-ph].

[14] J. Racker, M. Pena, and N. Rius, Leptogenesis with small violation of B-L, JCAP **1207**, 030, arXiv:1205.1948 [hep-ph].

[15] K. Moffat, S. Pascoli, S. T. Petcov, and J. Turner, Leptogenesis from Low Energy *CP* Violation, (2018), arXiv:1809.08251 [hep-ph].

[16] J. D. Clarke, R. Foot, and R. R. Volkas, Natural leptogenesis and neutrino masses with two Higgs doublets, Phys. Rev. **D92**, 033006 (2015), arXiv:1505.05744 [hep-ph].

[17] J. D. Clarke and R. R. Volkas, Technically natural nonsupersymmetric model of neutrino masses, baryogenesis, the strong CP problem, and dark matter, Phys. Rev. **D93**, 035001 (2016), [Phys. Rev.D93,035001(2016)], arXiv:1509.07243 [hep-ph].

[18] S. Weinberg, Cosmological Constraints on the Scale of Supersymmetry Breaking, Phys. Rev. Lett. **48**, 1303 (1982).

[19] H. Baer, S. Kraml, A. Lessa, and S. Sekmen, Thermal leptogenesis and the gravitino problem in the Asaka-Yanagida axion/axino dark matter scenario, JCAP **1104**, 039, arXiv:1012.3769 [hep-ph].

[20] H. Baer, S. Kraml, A. Lessa, and S. Sekmen, Reconciling thermal leptogenesis with the gravitino problem in SUSY models with mixed axion/axino dark matter, JCAP **1011**, 040, arXiv:1009.2959 [hep-ph].

[21] A. Pilaftsis and T. E. J. Underwood, Resonant leptogenesis, Nucl. Phys. **B692**, 303 (2004),

arXiv:hep-ph/0309342 [hep-ph].

[22] A. Pilaftsis and T. E. J. Underwood, Electroweak-scale resonant leptogenesis, *Phys. Rev.* **D72**, 113001 (2005), arXiv:hep-ph/0506107 [hep-ph].

[23] D. Wyler and L. Wolfenstein, Massless Neutrinos in Left-Right Symmetric Models, *Nucl. Phys.* **B218**, 205 (1983).

[24] C. N. Leung and S. T. Petcov, A Comment on the Coexistence of Dirac and Majorana Massive Neutrinos, *Phys. Lett.* **125B**, 461 (1983).

[25] R. N. Mohapatra, Mechanism for Understanding Small Neutrino Mass in Superstring Theories, *Phys. Rev. Lett.* **56**, 561 (1986).

[26] R. N. Mohapatra and J. W. F. Valle, Neutrino Mass and Baryon Number Nonconservation in Superstring Models, *Proceedings, 23RD International Conference on High Energy Physics, JULY 16-23, 1986, Berkeley, CA*, *Phys. Rev.* **D34**, 1642 (1986).

[27] E. Ma, Lepton Number Nonconservation in $E(6)$ Superstring Models, *Phys. Lett.* **B191**, 287 (1987).

[28] M. C. Gonzalez-Garcia and J. W. F. Valle, Fast Decaying Neutrinos and Observable Flavor Violation in a New Class of Majoron Models, *Phys. Lett.* **B216**, 360 (1989).

[29] M. C. Gonzalez-Garcia, A. Santamaria, and J. W. F. Valle, Isosinglet Neutral Heavy Lepton Production in Z Decays and Neutrino Mass, *Nucl. Phys.* **B342**, 108 (1990).

[30] F. Deppisch and J. W. F. Valle, Enhanced lepton flavor violation in the supersymmetric inverse seesaw model, *Phys. Rev.* **D72**, 036001 (2005), arXiv:hep-ph/0406040 [hep-ph].

[31] E. K. Akhmedov, M. Lindner, E. Schnapka, and J. W. F. Valle, Dynamical left-right symmetry breaking, *Phys. Rev.* **D53**, 2752 (1996), arXiv:hep-ph/9509255 [hep-ph].

[32] S. M. Barr, A Different seesaw formula for neutrino masses, *Phys. Rev. Lett.* **92**, 101601 (2004), arXiv:hep-ph/0309152 [hep-ph].

[33] M. Malinsky, J. C. Romao, and J. W. F. Valle, Novel supersymmetric $SO(10)$ seesaw mechanism, *Phys. Rev. Lett.* **95**, 161801 (2005), arXiv:hep-ph/0506296 [hep-ph].

[34] C. O. Dib, G. R. Moreno, and N. A. Neill, Neutrinos with a linear seesaw mechanism in a scenario of gauged B-L symmetry, *Phys. Rev.* **D90**, 113003 (2014), arXiv:1409.1868 [hep-ph].

[35] E. Ma, Deciphering the Seesaw Nature of Neutrino Mass from Unitarity Violation, *Mod. Phys. Lett.* **A24**, 2161 (2009), arXiv:0904.1580 [hep-ph].

[36] J. C. Pati and A. Salam, Lepton Number as the Fourth Color, *Phys. Rev.* **D10**, 275 (1974),

[Erratum: Phys. Rev. D11,703(1975)].

[37] R. N. Mohapatra and J. C. Pati, Left-Right Gauge Symmetry and an Isoconjugate Model of CP Violation, Phys. Rev. **D11**, 566 (1975).

[38] G. Senjanovic and R. N. Mohapatra, Exact Left-Right Symmetry and Spontaneous Violation of Parity, Phys. Rev. **D12**, 1502 (1975).

[39] R. N. Mohapatra and G. Senjanovic, Neutrino Masses and Mixings in Gauge Models with Spontaneous Parity Violation, Phys. Rev. **D23**, 165 (1981).

[40] A. Pilaftsis, Heavy Majorana neutrinos and baryogenesis, Int. J. Mod. Phys. **A14**, 1811 (1999), arXiv:hep-ph/9812256 [hep-ph].

[41] P.-H. Gu and U. Sarkar, Leptogenesis with Linear, Inverse or Double Seesaw, Phys. Lett. **B694**, 226 (2011), arXiv:1007.2323 [hep-ph].

[42] S. Blanchet, P. S. B. Dev, and R. N. Mohapatra, Leptogenesis with TeV Scale Inverse Seesaw in SO(10), Phys. Rev. **D82**, 115025 (2010), arXiv:1010.1471 [hep-ph].

[43] M. J. Dolan, T. P. Dutka, and R. R. Volkas, Dirac-Phase Thermal Leptogenesis in the extended Type-I Seesaw Model, JCAP **1806** (06), 012, arXiv:1802.08373 [hep-ph].

[44] K. Agashe, P. Du, M. Ekhterachian, C. S. Fong, S. Hong, and L. Vecchi, Hybrid seesaw leptogenesis and TeV singlets, Phys. Lett. **B785**, 489 (2018), arXiv:1804.06847 [hep-ph].

[45] K. Agashe, P. Du, M. Ekhterachian, C. S. Fong, S. Hong, and L. Vecchi, Natural Seesaw and Leptogenesis from Hybrid of High-Scale Type I and TeV-Scale Inverse, (2018), arXiv:1812.08204 [hep-ph].

[46] V. Cirigliano, B. Grinstein, G. Isidori, and M. B. Wise, Minimal flavor violation in the lepton sector, Nucl. Phys. **B728**, 121 (2005), arXiv:hep-ph/0507001 [hep-ph].

[47] D. N. Dinh, L. Merlo, S. T. Petcov, and R. Vega-Álvarez, Revisiting Minimal Lepton Flavour Violation in the Light of Leptonic CP Violation, JHEP **07**, 089, arXiv:1705.09284 [hep-ph].

[48] R. S. Chivukula and H. Georgi, Composite Technicolor Standard Model, Phys. Lett. **B188**, 99 (1987).

[49] A. J. Buras, P. Gambino, M. Gorbahn, S. Jager, and L. Silvestrini, Universal unitarity triangle and physics beyond the standard model, Phys. Lett. **B500**, 161 (2001), arXiv:hep-ph/0007085 [hep-ph].

[50] G. D'Ambrosio, G. F. Giudice, G. Isidori, and A. Strumia, Minimal flavor violation: An Effective field theory approach, Nucl. Phys. **B645**, 155 (2002), arXiv:hep-ph/0207036 [hep-ph].

ph].

- [51] L. Merlo and S. Rosauro-Alcaraz, Predictive Leptogenesis from Minimal Lepton Flavour Violation, *JHEP* **07**, 036, arXiv:1801.03937 [hep-ph].
- [52] V. Cirigliano, G. Isidori, and V. Porretti, CP violation and Leptogenesis in models with Minimal Lepton Flavour Violation, *Nucl. Phys.* **B763**, 228 (2007), arXiv:hep-ph/0607068 [hep-ph].
- [53] G. C. Branco, A. J. Buras, S. Jager, S. Uhlig, and A. Weiler, Another look at minimal lepton flavour violation, $l_i \rightarrow l_j \gamma$, leptogenesis, and the ratio M_ν/Λ_{LFV} , *JHEP* **09**, 004, arXiv:hep-ph/0609067 [hep-ph].
- [54] V. Cirigliano, A. De Simone, G. Isidori, I. Masina, and A. Riotto, Quantum Resonant Leptogenesis and Minimal Lepton Flavour Violation, *JCAP* **0801**, 004, arXiv:0711.0778 [hep-ph].
- [55] P. S. Bhupal Dev, P. Millington, A. Pilaftsis, and D. Teresi, Flavour Covariant Transport Equations: an Application to Resonant Leptogenesis, *Nucl. Phys.* **B886**, 569 (2014), arXiv:1404.1003 [hep-ph].
- [56] P. S. B. Dev, P. Millington, A. Pilaftsis, and D. Teresi, Corrigendum to "Flavour Covariant Transport Equations: an Application to Resonant Leptogenesis", *Nucl. Phys.* **B897**, 749 (2015), arXiv:1504.07640 [hep-ph].
- [57] A. Pilaftsis and D. Teresi, Mass bounds on light and heavy neutrinos from radiative minimal-flavor-violation leptogenesis, *Phys. Rev.* **D92**, 085016 (2015), arXiv:1506.08124 [hep-ph].
- [58] M. B. Gavela, T. Hambye, D. Hernandez, and P. Hernandez, Minimal Flavour Seesaw Models, *JHEP* **09**, 038, arXiv:0906.1461 [hep-ph].
- [59] S. Pascoli, S. T. Petcov, and A. Riotto, Connecting low energy leptonic CP-violation to leptogenesis, *Phys. Rev.* **D75**, 083511 (2007), arXiv:hep-ph/0609125 [hep-ph].
- [60] S. Pascoli, S. T. Petcov, and A. Riotto, Leptogenesis and Low Energy CP Violation in Neutrino Physics, *Nucl. Phys.* **B774**, 1 (2007), arXiv:hep-ph/0611338 [hep-ph].
- [61] A. Anisimov, S. Blanchet, and P. Di Bari, Viability of Dirac phase leptogenesis, *JCAP* **0804**, 033, arXiv:0707.3024 [hep-ph].
- [62] R. Alonso de Pablo, *Dynamical Yukawa Couplings*, Ph.D. thesis, Madrid, Autonoma U. (2013), arXiv:1307.1904 [hep-ph].
- [63] G. Isidori, Flavor physics and CP violation, in *Proceedings, 2012 European School of High-Energy Physics (ESHEP 2012): La Pommeraye, Anjou, France, June 06-19, 2012* (2014) pp. 69–105, arXiv:1302.0661 [hep-ph].

[64] T. Hurth, G. Isidori, J. F. Kamenik, and F. Mescia, Constraints on New Physics in MFV models: A Model-independent analysis of $\Delta F = 1$ processes, *Nucl. Phys.* **B808**, 326 (2009), arXiv:0807.5039 [hep-ph].

[65] G. Isidori, Y. Nir, and G. Perez, Flavor Physics Constraints for Physics Beyond the Standard Model, *Ann. Rev. Nucl. Part. Sci.* **60**, 355 (2010), arXiv:1002.0900 [hep-ph].

[66] T. Hurth and F. Mahmoudi, The Minimal Flavour Violation benchmark in view of the latest LHCb data, *Nucl. Phys.* **B865**, 461 (2012), arXiv:1207.0688 [hep-ph].

[67] A. Crivellin and L. Mercolli, $B^- \rightarrow X_d \gamma$ and constraints on new physics, *Phys. Rev.* **D84**, 114005 (2011), arXiv:1106.5499 [hep-ph].

[68] V. Khachatryan *et al.* (LHCb, CMS), Observation of the rare $B_s^0 \rightarrow \mu^+ \mu^-$ decay from the combined analysis of CMS and LHCb data, *Nature* **522**, 68 (2015), arXiv:1411.4413 [hep-ex].

[69] M. Tanabashi *et al.* (Particle Data Group), Review of Particle Physics, *Phys. Rev.* **D98**, 030001 (2018).

[70] S. Watanuki *et al.*, Measurements of isospin asymmetry and difference of direct CP asymmetries in inclusive $B \rightarrow X_s \gamma$ decays, in *39th International Conference on High Energy Physics (ICHEP 2018) Seoul, Gangnam-Gu, Korea, Republic of, July 4-11, 2018* (2018) arXiv:1807.04236 [hep-ex].

[71] *Study of the rare decays of $B0s$ and $B0$ into muon pairs from data collected during 2015 and 2016 with the ATLAS detector*, Tech. Rep. ATLAS-CONF-2018-046 (CERN, Geneva, 2018).

[72] S. Davidson and F. Palorini, Various definitions of Minimal Flavour Violation for Leptons, *Phys. Lett.* **B642**, 72 (2006), arXiv:hep-ph/0607329 [hep-ph].

[73] R. Alonso, G. Isidori, L. Merlo, L. A. Munoz, and E. Nardi, Minimal flavour violation extensions of the seesaw, *JHEP* **06**, 037, arXiv:1103.5461 [hep-ph].

[74] I. Esteban, M. C. Gonzalez-Garcia, A. Hernandez-Cabezudo, M. Maltoni, and T. Schwetz, Global analysis of three-flavour neutrino oscillations: synergies and tensions in the determination of θ_{23} , δ_{CP} , and the mass ordering, (2018), arXiv:1811.05487 [hep-ph].

[75] R. Alonso, M. B. Gavela, D. Hernandez, and L. Merlo, On the Potential of Leptonic Minimal Flavour Violation, *Phys. Lett.* **B715**, 194 (2012), arXiv:1206.3167 [hep-ph].

[76] R. Alonso, M. B. Gavela, D. Hernández, L. Merlo, and S. Rigolin, Leptonic Dynamical Yukawa Couplings, *JHEP* **08**, 069, arXiv:1306.5922 [hep-ph].

[77] R. Alonso, M. B. Gavela, G. Isidori, and L. Maiani, Neutrino Mixing and Masses from a

Minimum Principle, JHEP **11**, 187, arXiv:1306.5927 [hep-ph].

[78] S. Uhlig, Minimal Lepton Flavour Violation and Leptogenesis with exclusively low-energy CP Violation, JHEP **11**, 066, arXiv:hep-ph/0612262 [hep-ph].

[79] A. Abada, S. Davidson, A. Ibarra, F. X. Josse-Michaux, M. Losada, and A. Riotto, Flavour Matters in Leptogenesis, JHEP **09**, 010, arXiv:hep-ph/0605281 [hep-ph].

[80] B. Adhikary, M. Chakraborty, and A. Ghosal, Flavored leptogenesis with quasidegenerate neutrinos in a broken cyclic symmetric model, Phys. Rev. **D93**, 113001 (2016), arXiv:1407.6173 [hep-ph].

[81] J. A. Harvey and M. S. Turner, Cosmological baryon and lepton number in the presence of electroweak fermion number violation, Phys. Rev. **D42**, 3344 (1990).

[82] F. F. Deppisch and A. Pilaftsis, Lepton Flavour Violation and theta(13) in Minimal Resonant Leptogenesis, Phys. Rev. **D83**, 076007 (2011), arXiv:1012.1834 [hep-ph].

[83] V. Cirigliano and B. Grinstein, Phenomenology of minimal lepton flavor violation, Nucl. Phys. **B752**, 18 (2006), arXiv:hep-ph/0601111 [hep-ph].

[84] P. S. B. Dev and A. Pilaftsis, Minimal Radiative Neutrino Mass Mechanism for Inverse Seesaw Models, Phys. Rev. **D86**, 113001 (2012), arXiv:1209.4051 [hep-ph].

[85] J. A. Casas and A. Ibarra, Oscillating neutrinos and muon \rightarrow e, gamma, Nucl. Phys. **B618**, 171 (2001), arXiv:hep-ph/0103065 [hep-ph].

[86] D. Borah, M. K. Das, and A. Mukherjee, Common Origin of Non-zero θ_{13} and Baryon Asymmetry of the Universe in a TeV scale Seesaw Model with A_4 Flavour Symmetry, (2017), arXiv:1711.02445 [hep-ph].

[87] S. Blanchet, T. Hambye, and F.-X. Josse-Michaux, Reconciling leptogenesis with observable mu \rightarrow e gamma rates, JHEP **04**, 023, arXiv:0912.3153 [hep-ph].

[88] T. Hambye, J. March-Russell, and S. M. West, TeV scale resonant leptogenesis from supersymmetry breaking, JHEP **07**, 070, arXiv:hep-ph/0403183 [hep-ph].

[89] A. M. Baldini *et al.* (MEG), Search for the lepton flavour violating decay $\mu^+ \rightarrow e^+ \gamma$ with the full dataset of the MEG experiment, Eur. Phys. J. **C76**, 434 (2016), arXiv:1605.05081 [hep-ex].

[90] P. W. Cattaneo (MEG II), The MEGII detector, *Proceedings, International Conference on Instrumentation for Colliding Beam Physics (INSTR17): Novosibirsk, Russia*, JINST **12** (06), C06022, arXiv:1705.10224 [physics.ins-det].